



This is to certify that the

dissertation entitled

ULTRASONIC MATERIAL CHARACTERIZATION AND IMAGING BY UNSUPERVISED LEARNING

presented by

Jeng Tzong Sheu

has been accepted towards fulfillment of the requirements for

Ph.D. degree in <u>Electrical</u> Engineering

Major professor

Date 5/25/94.

LIBRARY Michigan State University

REMOTE STORAGE <a>R <a>R<

PLACE IN RETURN BOX to remove this checkout from your record. **TO AVOID FINES** return on or before date due.

DATE DUE	DATE DUE	DATE DUE
APR 238 2018		
AFIN LO ZOTO		

2/17 20# Blue FORMS/DateDueForms_2017.indd - pg.5

ULTRASONIC MATERIAL CHARACTERIZATION AND IMAGING BY UNSUPERVISED LEARNING

By Jeng Tzong Sheu

A DISSERTATION

Submitted to
Michigan State University
in partial fulfillment of requirements
for the degree of

DOCTOR OF PHILOSOPHY

Department of Electrical Engineering

1994

ABSTRACT

ULTRASONIC MATERIAL CHARACTERIZATION AND IMAGING BY UNSUPERVISED LEARNING

By

Jeng Tzong Sheu

Attenuation coefficient has been considered as a very important feature in biological tissues characterization. It is also a well-known fact that attenuation coefficient is strongly frequency dependent. However, estimation of attenuation coefficient of dispersive material is a very difficult task. Unlike traditional estimation methods, the proposed approach extracted material dependent features from echoes for qualitative analysis by unsupervised learning technique. Two unsupervised learning (clustering) algorithms and two cluster validity indices were evaluated by Monte Carlo study to obtain the statistical information. Finally, an algorithm and an index, according to the result of Monte Carlo study, were chosen to employ in the application of ultrasonic material characterization. The algorithm was implemented by the competitive learning model of artificial neural networks. The clustering results are represented in the form of images in which different color shades represents different clusters. Different data sets including data extracted from a phantom and a slice of brain sample were used in the experiments. The proposed method achieved some results which are very difficult to fulfill by traditional methods.

In loving memory of my mother

ACKNOWLEDGEMENTS

I sincerely thank Dr. B. Ho, my advisor, for his support, constant guidance, encouragement, and inspiring suggestions and discussions during the course of this study.

I would also give my thanks to the guidance committee members, Dr. R. Zapp, Professor J. Hall, and Professor L. Ni for taking time to serve in the committee.

Finally, I would like to thank my wife Chia-Hui and my daughter Sunny for their patience, love, and joy with me.

TABLE OF CONTENTS

LIST OF T	ABLE	S.S.	vii
LIST OF F	IGUR	ES	viii
Chapter 1	1.0	Introduction	1
	1.1	Overview	1
		1.1.1 Nondestructive evaluation by ultrasound	3
		1.1.2 Biomedical ultrasound	4
		1.1.3 Artificial neural networks	6
	1.2		7
	1.3	Thesis organization	8
Chapter 2	2.0	Background	9
	2.1	Linear acoustics	9
	2.2	Transmission, reflection, and attenuation coefficients	12
	2.3	Neural networks for unsupervised learning	15
		2.3.1 Competitive learning networks	18
		2.3.2 Kohonen's feature map	20
Chapter 3	3.0	Time-domain and Frequency-domain Techniques	22
•	3.1	Dual-interrogation technique	22
		3.1.1 Theoretical background	23
		3.1.2 Advantages and limitations	32
	3.2	Frequency domain technique	35
Chapter 4	4.0	Material Characterization Using Unsupervised Learning	41
•	4.1	• • • • • • • • • • • • • • • • • • • •	41
	4.2	Theoretical background	43
	4.3	Feature extraction	46
	4.4	Competitive unsupervised learning using neural networks	49
		4.4.1 Training algorithms	51
		4.4.1.1 Cluster validity	58
		4.4.2 Modified K-means algorithm using competitive	
		learning	60
		4.4.2.1 Cluster validity	64

Chapter 5	5.0	Simulation and Experimental Results	66
	5.1	Experimental results of time domain method	56
	5.2	Comparison of two algorithms and two indices	78
	5.3	Ultrasonic material characterization	85
Chapter 6	6.0	Conclusions	94
-	6.1	Summary	94
	6.2	Future work	95
BIBLIOGR	'APH'	Y	97

LIST OF TABLES

Table 1.1	A comparison between modern techniques	2
Table 1.2	Characteristics of neural networks and conventional computers	6
Table 5.1	Single layer of plexiglass (W-P-W), Thickness = 17.02 ± 0.01 mm	72
Table 5.2	Single layer of aluminum (W-A-W), Thickness = 12.70 ± 0.01 mm	73
Table 5.3	Three layers, plexiglass-water-plexiglass (W-P-W-P-W), Thickness: 11.02, 9.25, 7.02±0.01 mm	77
Table 5.4	Errors in estimating number of clusters using S, 100 patterns, spread=0.01, overlap=0.1, spherical window	81
Table 5.5	Errors in estimating number of clusters using MH, 100 patterns, spread=0.01, overlap=0.1, spherical window	82
Table 5.6	Errors in estimating number of clusters using S, 100 patterns, spread=0.1, overlap=0.3, spherical window	83
Table 5.7	Errors in estimating number of clusters using MH, 100 patterns, spread=0.1, overlap=0.3, spherical window	84

LIST OF FIGURES

Figure 1.1	Setup of basic ultrasound system	2
Figure 2.1	Acoustic wave at interface of different media with different impedance	12
Figure 2.2	Neuron of McCulloch and Pitts' model	16
Figure 2.3	Transfer functions of neurons	17
Figure 2.4	Architecture of competitive learning networks	18
Figure 2.5	Architecture of two-dimensional Kohonen's feature map	21
Figure 3.1	Bidirectional interrogation for N layered model	24
Figure 3.2	Reverberation paths of bidirectional interrogation	24
Figure 3.3	The impulse response pairs of dual interrogation	27
Figure 3.4	Multiple reflections of layer i	29
Figure 3.5	Experimental setup for incident signal measurement	33
Figure 3.6	Structure of multi-layered model for frequency domain method	37
Figure 4.1	System diagram	44
Figure 4.2	Stages of unsupervised learning	45
Figure 4.3	The three features in spectrum of echo signal	48
Figure 4.4	Demonstration of dead units problem. (a). A two-feature four clusters data set. (b). Result with a dead unit. (c). Result of MFSCL algorithm	52
Figure 4.5	Comparison of clustering results when size of clusters are different with same initial weight vectors, training sequence and learning rate. (a). Results of MSFCL method. (b). Results of FSCL method	55
Figure 4.6	(a). Convergence comparison between MFSCL, FSCL, and KSFM methods using well clustered data set. (b). Convergence comparison between MFSCL, FSCL, and KSFM methods using weak clustered data set. (c). Display of well clustered data set. (d). Display of weak clustered data set	56
Figure 4.7	(a). Configuration of competitive neural network with n clusters and five features. (b). Function of single neuron	62

Figure 4.8	Cost value v.s. number of clusters	65
Figure 5.1	Experimental setup of bidirectional interrogation	67
Figure 5.2	Reflection signals of single layer plexiglass in water. (a). Left-sided reflections. (b). Right-sided reflections	68
Figure 5.3	Transmission signals of single layer plexiglass in water. (a). left to right transmission signal. (b). Right to left transmission signal	69
Figure 5.4	Reflection signals of single layer aluminum in water. (a). Left-sided reflection signals. (b). right-sided reflection signals.	70
Figure 5.5	Fransmission signals of single layer aluminum in water. (a) left to right transmission signal. (b). Right to left transmission signal	71
Figure 5.6	Multiple reflections elimination. (a). Left-sided reflections. (b). Left-sided signals after multiple reflections elimination.	74
Figure 5.7	Reflection signals of multi-layered model. (a). Left-sided reflections. (b). Right-sided reflections	75
Figure 5.8	Transmission signals of multi-layered model. (a). Left to right transmission signal. (b). Right to left transmission signal	76
Figure 5.9	Modified Hubert's Gamma index v.s. number of clusters plot for different data sets.	87
Figure 5.10	(a). top view of phantom. (b). Phantom covered with plexiglass plate	88
Figure 5.11	Linear projection of five features onto two-dimensional space	89
Figure 5.12	Images of phantom. (a). C-scan image. (b). Reconstructed image when segmented data set into two clusters. (c). Three clusters. (d). Four clusters	90
Figure 5.13	Images of phantom covered with plexiglass plate. (a). C-scan image. (b). Reconstructed image when segmented data set into two clusters. (c). Three clusters. (d). Four clusters	91
Figure 5.14	Picture of human brain sample with hemorrhaged tumor	92
-	Images of human brain sample with hemorrhaged tumor. (a). C-scan image. (b). Reconstructed image when segmented data set into two clusters. (c). Three clusters. (d). Four clusters. (e) five clusters. (f). Six clusters	93

Chapter 1

1.0 Introduction

Ultrasonic techniques for nondestructive investigation have existed for a long period of time. But some of their limitations are still troublesome for many applications. It is the reason of this research to present an alternate approach in dealing with attenuation estimation problems quantitatively by using artificial neural networks (ANNs).

This chapter begins with brief overview of ultrasonic techniques and the fundamentals of neural networks. The problem to be solved and research tasks are then stated. Finally, the organization of chapters is outlined.

1.1 Overview

Ultrasonic techniques have wide variety of applications like in areas such as clinical diagnostics [1], non-destructive evaluations [14] (NDE), and many others [16]. The attractive features of using ultrasound are that it can probe the target without resorting to any destructive process, provides safety of operation, and acquire low examination cost as compared with the cost of other radiological media. Although magnetic resonance imaging (MRI), X-ray, and computer tomography (CT) outperformed ultrasound in image clarity, these techniques use short duration and high intensity electromagnetic (EM) energy emissions to penetrate the object to be examined. Cost of the equipment and the expense of examination are extremely high. At the present time, short-term and long-term exposure risks for both operator and living target are of great concerns. Instead of using

high energy EM source, ultrasound utilizes high frequency acoustic wave (stress wave) to interrogate the internal structures. So far, no evident has been reported related the operation risks for both the operators and targets. A comparison between these techniques is illustrated in Table 1-1.

A ultrasound system basically composed of following components: a *pulser* which generates high voltage short duration trigger pulse for triggering the transducer; transducers that can transform energy form between mechanical and electrical stimuli and responses; a *processing unit* to store acoustic signal and signal preprocessing for future use and display. Figure 1.1 shows the basic setup of a ultrasound system.

	-		<u>-</u>
Techniques	Cost of system	Image quality	Operation safety
MRI	Very High	Excellent	?
X-ray	Medium	Good	?
CT	High	Good	?
Ultrasound	Low	Poor	Yes

TABLE 1.1. A comparison between modern techniques.

Acoustic impedance, speed, and attenuation are important parameters for material and tissue characterization. In the past two decades, researchers put most of their efforts in obtaining the quantitative relationship between acoustic parameters and material properties and pathological changes in clinical environment. The applications in the nondestructive evaluation of materials are rather successful. However, in clinical evaluations a lot more are to be desired, as indicated in Table 1.1.

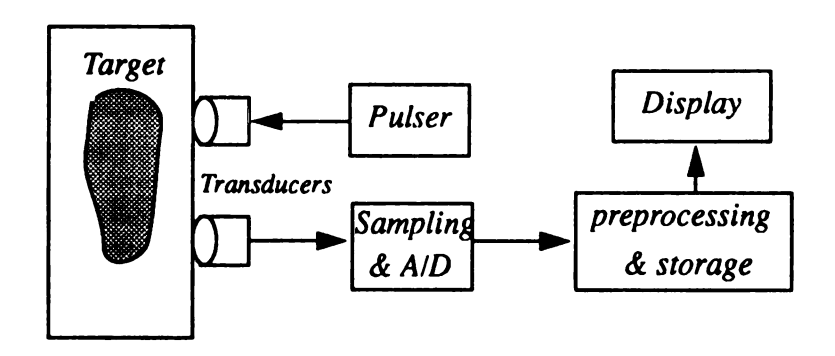


Figure 1.1 Setup of a basic ultrasound system.

1.1.1 Nondestructive Evaluation by Ultrasound

Nondestructive evaluation of materials by ultrasound has shown rapid growth in recent years, especially in the testing of composite materials which becomes a major construction material in both automotive and aerospace industries [16, 17, 29]. A great deal of information about the mechanical properties of material can be retrieved from the ultrasonic echo returns. However, in order to assure the success and consistency of nondestructive evaluation, the acoustical properties such as velocity, attenuation, reflection coefficient, etc. should be obtained with high reliability and accuracy.

For composite material, a common defects is the delamination between layers. Time-of-flight C-scan imaging technique can be used to display the amount of energy reflected from certain distance in depth of a given layer. Successful C-scan imaging systems have been implemented to display two dimensional images for defects and flaws inside composite materials [14].

Due to the ringing of ultrasonic pulsed signal and the complexity of the acoustic beam profile, the ultrasonic image quality is greatly deteriorated. A great deal of research efforts have been spent in improving the range resolution and lateral resolution for better image quality. Range resolution is the system ability to distinguish two different acoustic echoes in time sequence. When the thickness of individual layers are thin, overlapping of echoes from layer interfaces will occur. Theoretically, range resolution can be improved by using narrow transmitting pulses which can be provided by a broad-bandwidth and low-Q transducer. However, such transducers are not available due to the difficulties in fabrication technology. Various techniques have been proposed to improve the range resolution. Beretsky et.al., used frequency deconvolution to improve ultrasonic imaging[32]. Steiner et. al., proposed a generalized cross-correlation to improve resolution [33]. Yamada presented an on-line deconvolution for high resolution ultrasonic pulse-echo measurements under the constraints of narrow-band transducer [34]. Papoulis

et. al., demonstrated a repetitive algorithm to distinguish two overlapping pulse echoes by digital signal processing technique [37].

Lateral resolution is the ability to distinguish different nearby objects in the spatial domain. Owing to the inherent drawbacks of dispersive nature and physical size of acoustic beam, the lateral resolution of ultrasound system is highly hampered. Ho et. al., used correlation technique to improve the lateral resolution in C-scan imaging system [35]. Hundt, et, al., reported that improvement can be achieved by using digital filtering technique [36]. Yakota et. al., presented a method of firing transducer array repetitively to obtain an adaptive focusing effect [53].

1.1.2 Biomedical Ultrasound

Acoustic impedance, attenuation, and speed of different tissues have been investigated for more than two decades. Most of the work has been focused on getting quantitatively relationship between acoustic parameters and different tissues. Under some controlled environment and conditions, researchers did reach some significant results between pathological changes and acoustic responses. Among all the acoustic parameters, attenuation coefficient has been recognized as an important property in differentiating tissues [38]. In general, one can either use transmission or reflection techniques for biomedical applications. Transmission technique [3-6] for impedance and attenuation estimation was proposed first due to its simplicity and straightforward manner. Unfortunately, transmission technique suffers various drawbacks. Unlike X-ray, acoustic beam has much wider beam cross-sections and divergency. It can easily be defocused after it penetrates the biological structure. Greenleaf et. al., [7,39] used transmission technique to estimate the attenuation of lesions of breast tissues. The results were not very promising. R. Kuc et. al., [1, 43,45,47] proposed an approach to estimate the attenuation from reflected echoes on the assumption that attenuation coefficient is a strong function of frequency. Based on this assumption, two categories of approaches were presented to estimated attenuation coefficient. The spectral-shift approach estimates attenuation coefficient from the downshift of the echo spectra when comparing with that of the incident pulse. This method assumes the propagating pulse has a Gaussian-shaped spectrum. The spectral-difference method estimate attenuation coefficient from the change of slope between the near region and far region log spectra. This method does not require a specific form of spectra but suffers from marginal estimation accuracy due to bias errors from small scale size of data. Over the years, some researchers proposed time-domain methods [46,54,55] for attenuation estimation. Although time-domain methods provide straightforward and real-time processing ability, difficulties such as signal distortion from highly dispersive media and echoes overlapping are remain to be resolved. In addition, most of the time-domain methods require the use of narrow-band signal which is very difficult, if not impossible, to generate by a practical transducer. Recently, P. He et. al., [11,18,27] proposed envelope peak method by preprocessing the wide-band signal using the split spectrum technique [19-21] to obtain a bank of narrow-band signals. The attenuation is estimate from these narrow-band signals by time domain methods. Based on the methods described above both in vivo and in vitro measurements were conducted [9,20,42].

K. J. Parker et. al., [12,15,20,22] used statistical model to reduce the attenuation estimation errors by separating absorption and scattering factors for B-scan imaging system. P. S. Green [10,59] proposed a volumetric reflex transmission imaging system. This method basically is an extension of the conventional C-scan imaging technique by using annual array transducers to provide focal range for image display. It has the disadvantages of requiring huge storage space for data and its long processing time. Because of the difficulties in estimating acoustic parameters by traditional methods, images processing and pattern recognition techniques [23,25,26,60] were adopted to enhance the estimation results. But, almost all of these techniques were used in post-

processing stage. No fundamental improvement has been announced in biomedical applications.

1.1.3 Artificial Neural Networks

An ANNs is a parallel distributed information processing system which consists of neurons (processing elements) and synapses (connections). Each neuron, characterized by its own specific working function, receives and generates signals to a number of neurons via synapses. The function of an ANNs system depends on the structure of how neurons and synapses are connected. Since the outputs of an ANNs system are the result of cooperative work of all neurons, even though there may exist damages between connections, and faults from neurons the system can still produce significant results as long as the malfunction parts are not overwhelming. In other words, ANNs exhibits fault tolerance property. The other important feature of ANNs is its massive parallel computational ability which is essential for many applications requiring high computation capacity such as pattern recognition, and combinatorial optimization problems. Table 1-2 demonstrates the characteristics differences between neural networks and conventional digital computers [98].

TABLE 1.2. Characteristics of neural networks and conventional computers

Characteristics	Neural Networks	Conventional Computers
Memory Structure	Distributed	System-Dependent
Memory Access	Associative	Specific Input
Fault Tolerance	Inherent	Not Inherent
Pattern Recognition	Excellent	Poor
Classification	Excellent	Poor
Learning	Excellent	Poor
Arithmetic Capability	Poor	Excellent
Timing Scheme	Asynchronous	System-Dependent
Degree of Parallelism	High	System-Dependent
Degree of connectivity	High	Low
Processing Element	Simple	Complex

The ANNs architecture can basically be classified into two categories; recurrent networks and layer-structure networks. In recurrent network, each neuron has synapses connected to all others neurons including itself. Hopfield-Tank network [60] is the most well-known one of this type. In layer-type network, synapses only exist between consecutive layers or between peers. Multiple layer perceptron belongs to this type. Artificial neural network has been applied to traveling salesman problem [61, 62], linear programming [63], object recognition [64], and others [65, 66]. For ANNs, problems can be solved by designing and training an appropriate network whose minimum energy states correspond to the solutions of the given problem.

1.2 Objective and Research Tasks

Determination of materials (tissues) properties using ultrasound can be achieved by extracting acoustic parameters from reflected echoes or from transmission signals. Although there are numerous proposed methods for acoustical parameters estimations, quantitative scheme for characterizating inhomogeneous material is still not well developed. Echoes return from inhomogeneous material, especially biological tissues, are basically resulted from a collective scatters which are random in nature to the ultrasound beam. Estimation of the acoustical parameters of such targets is by no means an easy task.

Attenuation property has been recognized as an important feature for tissues characterization. It is a well-known fact that the attenuation coefficient is highly frequency dependent. In stead of solving the tissues characterization problem quantitatively, qualitative scheme should first be devised. Features related to attenuation coefficient in frequency domain are extracted from the echoes and constitute a pattern data set. Unsupervised learning (clustering) will then be applied to classify the data set into clusters. Different clusters represent different acoustical attenuation characteristics. To accomplish this, following steps are to be followed.

- (1) Time domain signals need to be sampled and stored in a clearness manner.
- (2) Range resolution and lateral resolution of the system have to be well calibrated and documented.
- (3) Develop an appropriate algorithm and forming an artificial neural networks for clustering analysis.

Images will then be reconstructed from the clustering information such that different color shades represent different clusters. In addition, image processing techniques can be applied to the clustering results to provide further spatial information.

1.3 Thesis Organization

The organization of this dissertation is as followed. Chapter 2 contains a background discussion of appropriate topics on ultrasound and artificial neural networks. In Chapter 3, both time domain acoustic parameters estimation method and frequency domain method are presented. Advantages and limitations are discussed.

Chapter 4 demonstrated the relationship between frequency response and attenuation.

Artificial neural networks for clustering will be presented. Algorithms are developed to perform the unsupervised learning using neural network.

Chapter 5 shows the experimental setup and results for the time domain method. Then, the Monte Carlo method is used to compare the algorithms. The images of clustering results for different samples are included in this chapter. Finally, conclusions, contributions, and suggested future research are stated in chapter 6.

Chapter 2

2.0 Background

This chapter begins with an introduction of the theory of linear plane acoustic wave. Then, some important acoustic parameters which are widely utilized for material characterization will be stated. Finally, models of artificial neural networks for unsupervised learning will be introduced.

2.1 Linear acoustics

In order to present the fundamental phenomena of linear acoustics, its loss mechanisms are ignored for simplicity. Furthermore, only on-dimensional plane wave is demonstrated here. In reality, there may exist different types of acoustic wave in a given system, such as longitudinal, shear, traverse etc. [68,69]. However, only the longitudinal wave is considered here since it is almost exclusively used in the areas of nondestructive evaluations of materials and clinical applications. Since acoustic wave is a mechanical wave (stress wave), it propagates via media. Pressure and particle velocity are two observable parameters of a propagating acoustic wave.

Assume that a homogeneous medium undergoes small departures from its rest state, the particle velocity and pressure are related by

$$\frac{\partial u}{\partial x} = \frac{-1}{k} \frac{\partial p}{\partial t} \tag{2.1}$$

and

$$\frac{\partial p}{\partial x} = -\rho \frac{\partial u}{\partial t} \tag{2.2}$$

where k is the coefficient of elasticity and ρ is the density of the medium.

Equation 2.1 is the mass continuity equation and the equation 2.2 is the momentum equation. From these two equations the acoustic plane wave equations can be obtained as

$$\frac{\partial^2 p}{\partial t^2} = \frac{k \partial^2 p}{\rho \partial x^2} \tag{2.3}$$

and

$$\frac{\partial^2 u}{\partial t^2} = \frac{k \partial^2 u}{\rho \partial x^2} \tag{2.4}$$

The general solution for the pressure and the particle velocity in the forward x-direction are

$$p = p(0) \exp(j(wt - Kx))$$
 (2.5)

$$u = u(0) \exp(j(wt - Kx))$$
 (2.6)

Where K is the wave number given by

$$K = \omega \sqrt{\frac{\rho}{k}} \quad . \tag{2.7}$$

In general, the wave number is a complex quantity. It consists of the phase constant β and the attenuation constant α ,

$$K = \beta - i\alpha \quad . \tag{2.8}$$

The relationship between pressure and the particle velocity can be derived from Equation 2.3, 2.5, and 2.6 as:

$$p = \frac{\omega \rho}{K} u \quad . \tag{2.9}$$

The characteristic acoustic impedance is defined as the ratio of the pressure to particle velocity,

$$Z \equiv \frac{p}{\mu} = \frac{\omega \rho}{K} \quad . \tag{2.10}$$

For a lossless homogeneous media, the phase velocity is

$$v_p = \frac{\omega}{K} = \frac{\omega}{\beta} \quad . \tag{2.11}$$

Therefore, the acoustic impedance for a lossless medium can be expressed as

$$Z = \rho v_{\rho} . \tag{2.12}$$

The evaluation of the velocity of propagating becomes rather complicated for a pulsed acoustic signal since it contains many frequency components and the medium is general dispersive in nature. A further complication comes from that the attenuation is also a strong function of frequency. As a result, the frequency spectral distribution will be altered when the wave is passing through a loosy medium. A more detail discussion of such situation will be given in later chapter.

2.2 Transmission, reflection, and attenuation coefficients

Material characterization using acoustic wave is mainly based on the detection of echo return from a material interface. It is therefore important to know how and where the wave being reflected back. Consider a plane wave is propagating from medium 1 to medium 2, as shown in Figure 2.1. By using the Snell's law and the continuity of both pressure and velocity at the boundary, we have

$$p_i + p_r = p_t \tag{2.13}$$

and

$$u_i \cos \theta_i - u_r \cos \theta_r = u_t \cos \theta_t \tag{2.14}$$

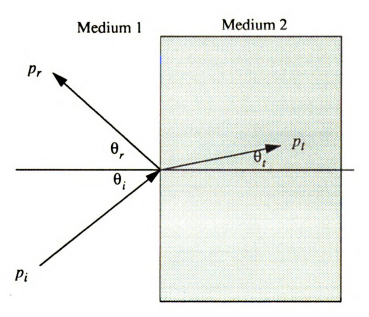


Figure 2.1 Acoustic wave at interface of different media with different acoustic impedance.

From Equation 2.9 and 2.14, we can obtain

$$\frac{p_i K_1 \cos \theta_i}{\rho_1} - \frac{p_r K_1 \cos \theta_r}{\rho_1} = \frac{p_t K_2 \cos \theta_t}{\rho_2} \quad . \tag{2.15}$$

By rearranging Eq. 2.15 using the terms in Eq. 2.13, the pressure reflection and transmission coefficients are

$$r = \frac{p_r}{p_i} = \frac{\frac{K_1}{\rho_1} \cos \theta_i - \frac{K_2}{\rho_2} \cos \theta_i}{\frac{K_1}{\rho_1} \cos \theta_i + \frac{K_2}{\rho_2} \cos \theta_i}$$
(2.16)

and

$$t = \frac{\rho_i}{\rho_i} = \frac{2\frac{K_2}{\rho_2}\cos\theta_i}{\frac{K_1}{\rho_1}\cos\theta_i + \frac{K_2}{\rho_2}\cos\theta_i} \qquad (2.17)$$

For normal incidence, i.e. $\theta_i = \theta_r = 0^\circ$, the reflection and transmission coefficients become

$$r = \frac{p_r}{p_i} = \frac{\frac{K_1}{\rho_1} - \frac{K_2}{\rho_2}}{\frac{K_1}{\rho_1} + \frac{K_2}{\rho_2}}$$
(2.18)

$$t = \frac{p_t}{p_i} = \frac{2\frac{K_2}{\rho_2}}{\frac{K_1}{\rho_1} + \frac{K_2}{\rho_2}} . \tag{2.19}$$

Using the acoustic impedance definition as given by Eq. 2.10, the reflection and transmission coefficients can be put in terms of the acoustic impedance of the two media as

$$r = \frac{Z_2 - Z_1}{Z_1 + Z_2} \tag{2.20}$$

$$t = \frac{2Z_2}{Z_1 + Z_2} = 1 + r . {(2.21)}$$

These coefficients are defined as the ratio of the pressures at the interface location. When considering pressure changes from one place to another, the effect of attenuation has to be taken into account. The attenuation phenomena of a travelling acoustic wave is a complicated one. Scattering and absorption all contribute to the attenuation of acoustic energy. The scattering effect causes some acoustic energy off the acoustic pathway, while the absorption results in heat generation. This is due to the fact that the density fluctuations in the medium is out of phase with the acoustic pressure fluctuations [67].

Attenuation measurement can be accomplished by either using time domain or frequency domain approach. Time domain technique requires a precise location of the pulse and its amplitude, while frequency domain requiring a broadband transducer. The accuracy of both techniques are highly limited by the measurement and the transducer fabrication technology available todate.

When a plane acoustic pressure wave propagating through a lossy medium, the amplitude of the acoustic pressure can be represented as

$$p(l) = p_0 exp(-\alpha(f)l)$$
 (2.22)

where p_0 is the initial pressure magnitude at a reference point, l is the distance travelled in the medium. Once p, p_0 , and l are known, $\alpha(f)$ can be determined. Unfortunately, the thickness of the layer is usually unknown, as a result, one can only obtain the $\alpha(f) \cdot l$ product. In chapter 3, time domain and frequency domain methods for attenuation estimation will be described in detail.

2.3 Neural networks for unsupervised learning

Neural networks incorporate a combination of features of information processing systems together with some special features. These features include the use of simple processing elements and learning abilities to adjust parameters and connection weights to give desired responses as well as to compensate for inaccuracies and faults in the hardware, and parallel processing ability. The use of simple processing elements can facilitate the fabrication of such parallel systems. The learning features provides a very important advantage in dealing with the detail knowledge necessary to build the system.

Neuron is the basic building block of a neural network. The simplest artificial neuron model was first introduced by McCulloch and Pitts [70]. The neuron output of the model is a function of the sums of weighted inputs. The model is shown in Figure 2.2. where X_i 's is the inputs from other neurons, W_{ij} is the weight of the connection from the output of neuron i to the neuron j, f(.) is the neuron transfer function, θ_j is the threshold value, and Y_j is the output of neuron j.

The transfer function of a neuron is commonly one of the three types: hardlimit, linear, and sigmoid functions. Their input/output relationship are shown in Figure 2.3. Different artificial neural networks can be achieved by interconnecting neurons in different ways

such that the networks have different training rules. In the following section, the basic function of neural networks which are applied in the realm of unsupervised are introduced.

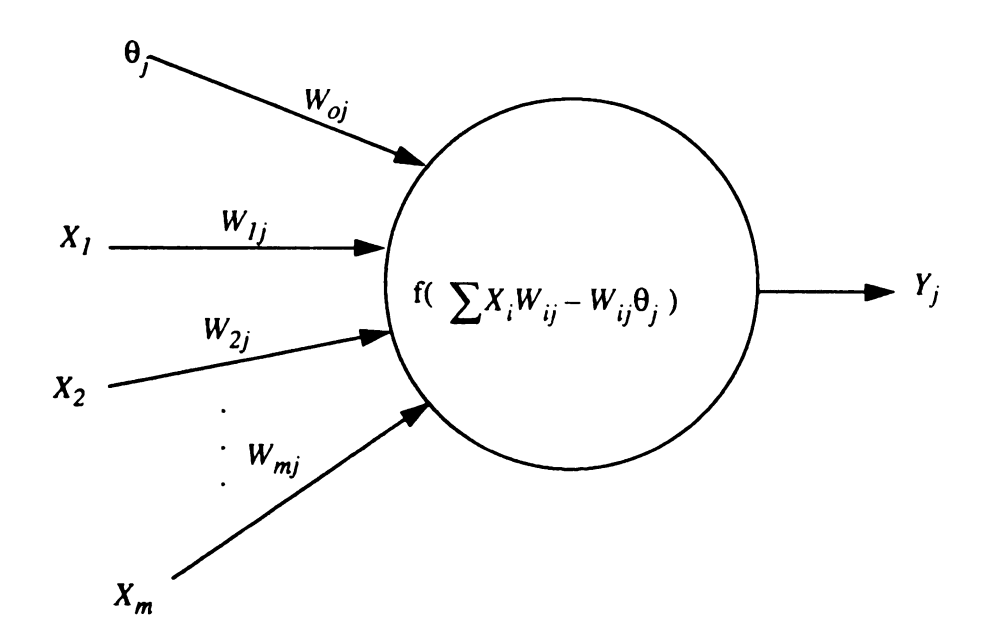
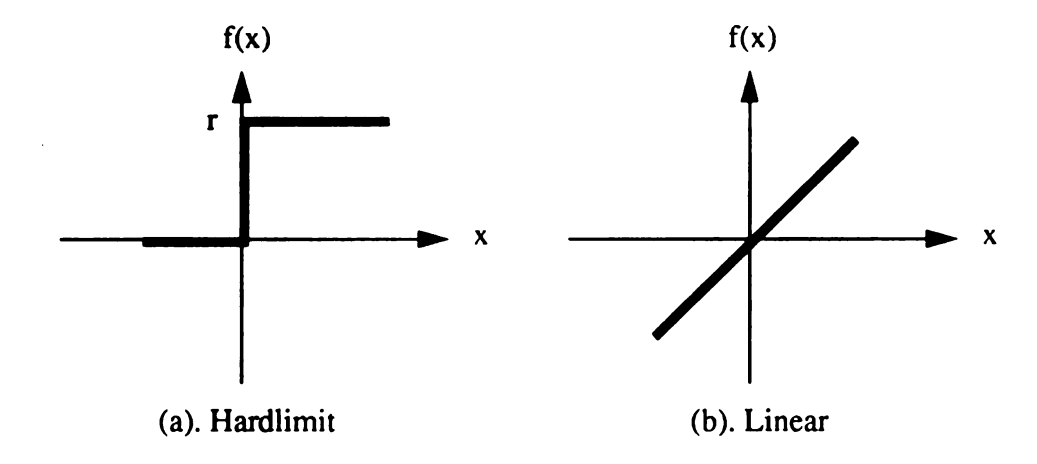


Figure 2.2 Neuron of McCulloch and Pitts' model.



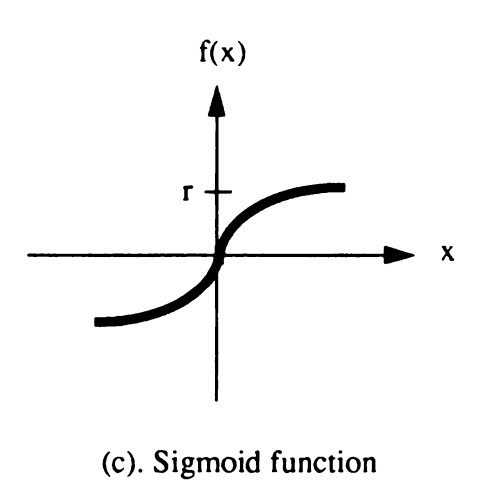


Figure 2.3 Transfer functions of neuron.

2.3.1 Competitive learning networks

In the competitive learning networks there is a single layer of output units Y_i , each fully connected to a set of inputs X_j via connections W_{ij} . Figure 2.4 shows the architecture of competitive learning networks. Only one of the output units, called the winner, can fire at a time. The winner is normally the unit with the largest net input

$$h_i = \sum_j W_{ij} X_j = W_i \cdot X \tag{2.23}$$

for the current input vector X. This is equivalent to

$$\left|W_{i} - X\right| \le \left|W_{j} - X\right| \tag{2.24}$$

for all $j \neq i$.

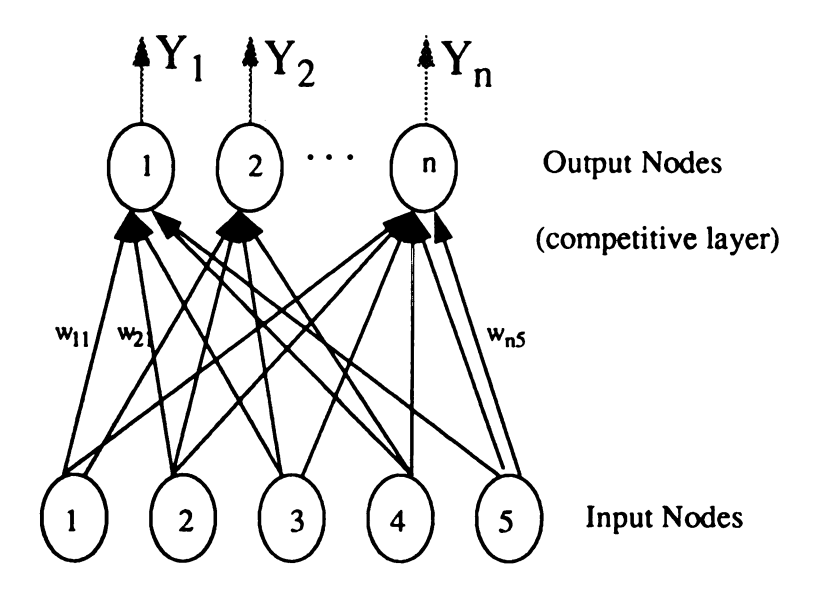


Figure 2.4 Architecture of competitive learning networks.

For each input pattern, we find the winner among the outputs and then update the weight W_{i*j} for the winning unit only to make the W_{i*} vector closer to the current input pattern. The updating rule is represented as

$$W_{i}(n+1) = W_{i}(n) + \eta (X - W_{i}(n)) Y_{i}$$
 (2.25)

where η is the learning rate, and is typically decreased monotonically to zero as the learning progresses.

According to the weight updating rule as described in Eq. 2.25, the cost (Lyapunov) function [71] can be written as

$$E\{W_{ij}\} = \frac{1}{2} \sum_{ij\mu} M_i^{\mu} \left(X_j^{\mu} - W_{ij}\right)^2 = \frac{1}{2} \sum_{\mu} \left|X^{\mu} - W_{i^{\circ}}\right|^2 . \tag{2.26}$$

 M_i^{μ} is the cluster membership matrix which specifies whether or not input pattern X^{μ} activates unit i as winner:

$$M_i^{\mu} = \left\{ \begin{array}{ll} 1 & \text{if } i = i^{\circ} (\mu) \\ 0 & , \text{otherwise} \end{array} \right. \tag{2.27}$$

Gradient descent on the cost function yields

$$\langle \Delta W_{ij} \rangle = -\eta \frac{\partial E}{\partial W_{ij}} = \eta \sum_{\mu} M_i^{\mu} \left(X_j^{\mu} - W_{ij} \right)$$
 (2.28)

which is just the sum of the updating rule over all patterns μ for which i is the winner. Thus, on average the updating rule will decreases until local minimum is reached if η is properly chosen.

The competitive learning network has two fundamental drawbacks; First, there is no guarantee of finding the global minimum. Many approaches were proposed to kick the system out of higher minimum and towards progressively lower ones. However, the problem remains. Second, in a competitive learning network, some neurons may never win during the whole learning training process. This is called the dead units problem. We will discuss this problem and deal with it in Chapter 4.

2.3.2 Kohonen's feature map

The KSFM networks [73] and the competitive learning networks are similar in weight updating rule. However, in the KSFM structure each neural unit has its topological neighborhood. During the training process, the weight vectors of the winning neuron as well as the weight vectors of its topological neighbors are all updated. The size of the neighborhood is decreased as the training progresses until the neighbor size equal to one. As a result, KSFM will become competitive learning after a certain epochs of training. The weight updating rule for neuron *i* and its neighborhood is

$$\Delta W_{ij} = \eta \Lambda (i, i^{\circ}) (X_j - W_{ij})$$
 (2.29)

for all i and j. The **neighborhood function** $\Lambda(i, i^{\circ})$ is 1 for $i = i^{\circ}$ and falls off with distance $|r_i - r_{i^{\circ}}|$ between units i and i° in the output array. According to the updating rule as described in Eq. 2.29, the cost function will be

$$E\{W_{ij}\} = \frac{1}{2} \sum_{ijk\mu} M_i^{\mu} \Lambda(i,k) \left(X_j^{\mu} - W_{ij}\right)^2 = \frac{1}{2} \sum_{i\mu} \Lambda(i,i^{\circ}) \left|X^{\mu} - W_{i^{\circ}}\right|^2 . \quad (2.30)$$

Again, M_i^{μ} is the cluster membership matrix. The gradient descent on this cost function yields

$$\langle \Delta W_{ij} \rangle = -\eta \frac{\partial E}{\partial W_{ij}} = \eta \sum_{\mu} M_i^{\mu} \Lambda(i, k) \left(X_j^{\mu} - W_{ij} \right)$$
 (2.31)

$$= \sum_{\mu} \Lambda (i, i^{\circ}) \left(X_{j}^{\mu} - W_{ij} \right) . \qquad (2.32)$$

This is just the sum of the Kohonen's rule over all patterns. Thus, on average (if η properly chosen) the Kohonen rule decreases the cost until we reach a local minimum. A detail comparison in computation time and convergence of networks based on competitive learning and Kohonen's models will be given in detail in Chapter 4. The architecture of 2-D Kohonen's feature map is shown in Figure 2.5.

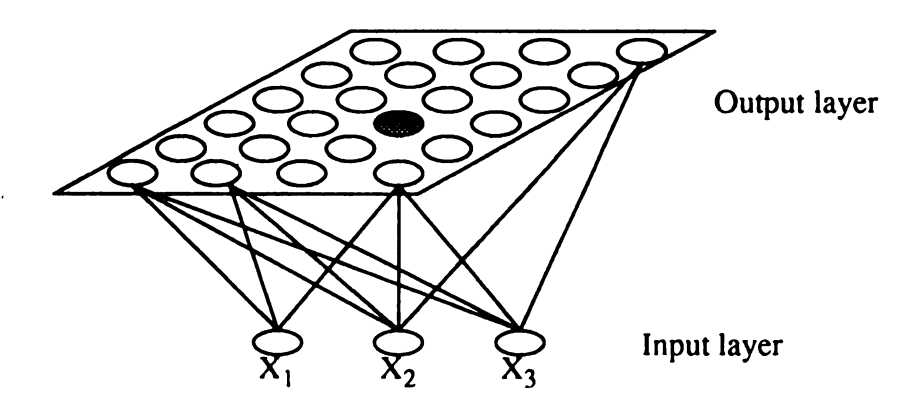


Figure 2.5 Architecture of two-dimensional Kohonen's Feature map.

Chapter 3

3.0 Time-domain and Frequency-domain Techniques

In this chapter time domain and frequency domain techniques for multi-layered model will be reviewed. The limitations and advantages of these approaches will also discussed.

3.1 Dual-interrogation technique

Noninvasive evaluation of material characteristics is now a well accepted tool for both clinical and industrial applications. To date, most of the systems are of reflection type. The reflected acoustic signal from an interface received and processed by the conventional pulse-echo technique, such as the B scan, is determined by the reflection coefficient at the interface as well as the attenuation of substance along the acoustic beam path. It is therefore impossible to retrieve these two type of information (attenuation and reflection) by the knowledge of a signal trace of echo return. Additional information is needed to evaluate the reflection coefficient and attenuation separately. A method proposed by Ho [74] and modified by the author is accomplished by using a second pulse-echo process from the opposite side of the object to furnish the necessary information.

Extensive work has been done on nondestructive evaluation of material properties by ultrasonics over the years. However, the conventional pulse-echo technique suffers from various drawbacks, such as the inability of evaluating material attenuation properties as those from X-ray tomography and the inherent limitation in resolution [74]. An ultrasound

signal reflected from the internal discontinuities of an object contains not only information about the reflection coefficient at the interface, but also the attenuation of the medium between the boundaries. It is practically impossible to separate the backscatter and attenuation from a single pulse echo return. Sophisticated techniques have been devised to estimate the attenuation property by assuming that the reflection coefficient at the discontinuity is either independent of frequency [75] or a simple linear function of frequency [1]. Other authors have relied upon a model with known relationship between successive interfaces [3]. A technique which is discussed in the following section allows the computation of a quantity relates the attenuation-velocity product of the medium and the reflection efficient at each interface in the medium from the experimental data is developed.

3.1.1 Theoretical Background

Consider the object under tested consists of homogeneous layers, the impulse response of the medium can be represented as

$$h(t) = \sum_{i} E_{i} \delta(t - t_{i})$$
 (3.1)

where t_i correspond to the locations of each reflecting surfaces. The quantity E_i in the equation includes the reflection and attenuation efforts. With this representation, the amplitude of each echo can be obtained directly from the A-mode echo return.

A simple one-dimensional model for bidirectional (dual) interrogation is shown in Figure 3.1. There are N layers of distinct materials comprising the model. On both sides, transducers are used for transmitting and receiving echoes during the measurements. The reverberation path of this multi-layered model is shown in Figure 3.2. When considering the reflection (or transmission) and attenuation effects in this model, the return echoes

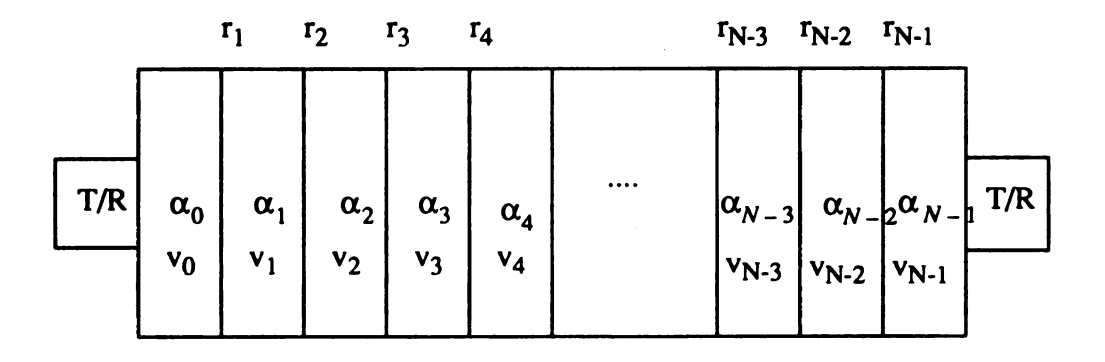


Figure 3.1. Bidirectional interrogation for N layered model.

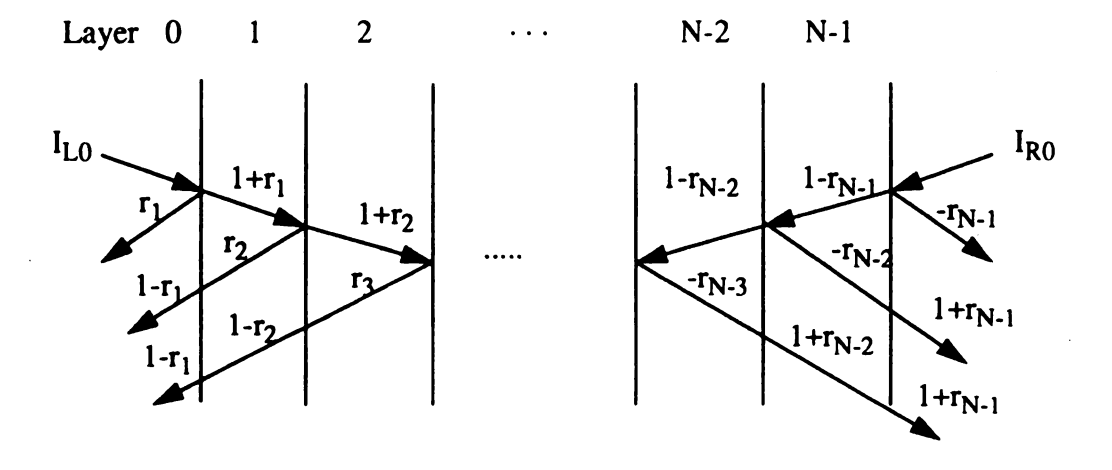


Figure 3.2. Reverberation paths of bidirectional interrogation.

from individual layers and the transmission signals through the object can be expressed in the following forms.

Echo received by the left transducer is

$$E_{Li}(k,r) = I_{L0}k_0^2 r_i \prod_{j=1}^{i-1} \left(1 - r_j^2\right) k_j^2 . \tag{3.2}$$

Echo received by the right transducer is

$$E_{Ri}(k,r) = I_{R0}k_i^2(-r_i) \prod_{j=i+1}^{N-1} \left(1 - r_j^2\right) k_j^2 . \tag{3.3}$$

Transmission signal from left to right is

$$T_{LR}(k,r) = I_{L0}k_0 \prod_{j=1}^{N-1} (1+r_j)k_j . (3.4)$$

Transmission signal from right to left is

$$T_{RL}(k,r)) = I_{R0}k_0 \prod_{j=1}^{N-1} (1-r_j)k_j$$
 (3.5)

where r_i is the reflection coefficient of layer i, I_{R0} and I_{L0} are the transmitting pulse amplitudes from the right and left transducers respectively, and k_i is the loss factor of layer i which can be expressed as

$$k_i = exp\left[-\alpha_i v_i t_i\right] \tag{3.6}$$

where α_i is the attenuation coefficient, v_i is the propagation velocity, and t_i is the propagation time delay of layer *i*. The impulse responses of dual interrogation is shown in Figure 3.3.

In this generalized model, the unknown quantities include N-1 values of r_i , N values of k_i , and the initial intensities I_{L0} and I_{R0} , a total of 2N+1 unknowns. Typically, the object is emerged in water, such that the loss factors k_0 and k_N become known quantities. The total number of unknowns are then reduced to 2N-1. From experimental data, we have N-1 echoes from the left receiver, and N-1 echoes from the right receiver. Adding the transmitted signals (T_{LR}, T_{RL}) , we have altogether 2N equations. The system is therefore solvable analytically. Two cases are considered here to obtain the attenuation-velocity product (αv) and the reflection coefficient (r) of all layers.

Case 1. Using both the reflected and transmitted signals

The product of Eqs. 3.2 and 3.3 can be put in terms of the product of equations 3.4 and 3.5 as follows.

$$E_{Li}(k,r)E_{Ri}(k,r) = T_{LR}(k,r)T_{RL}(k,r)\left[\frac{-r_i^2}{1-r_i^2}\right]$$
(3.7)

where i=1 to N-1.

The reflection coefficient of layer i can then be obtained as

$$r_{i} = \left(\frac{-E_{Li}(k,r)E_{Ri}(k,r)}{T_{LR}(k,r)T_{RL}(k,r) - E_{Li}(k,r)E_{Ri}(k,r)}\right)^{1/2}$$
(3.8)

After all reflection coefficients r_i are evaluated, the loss factor of each layer can be obtained as follows.

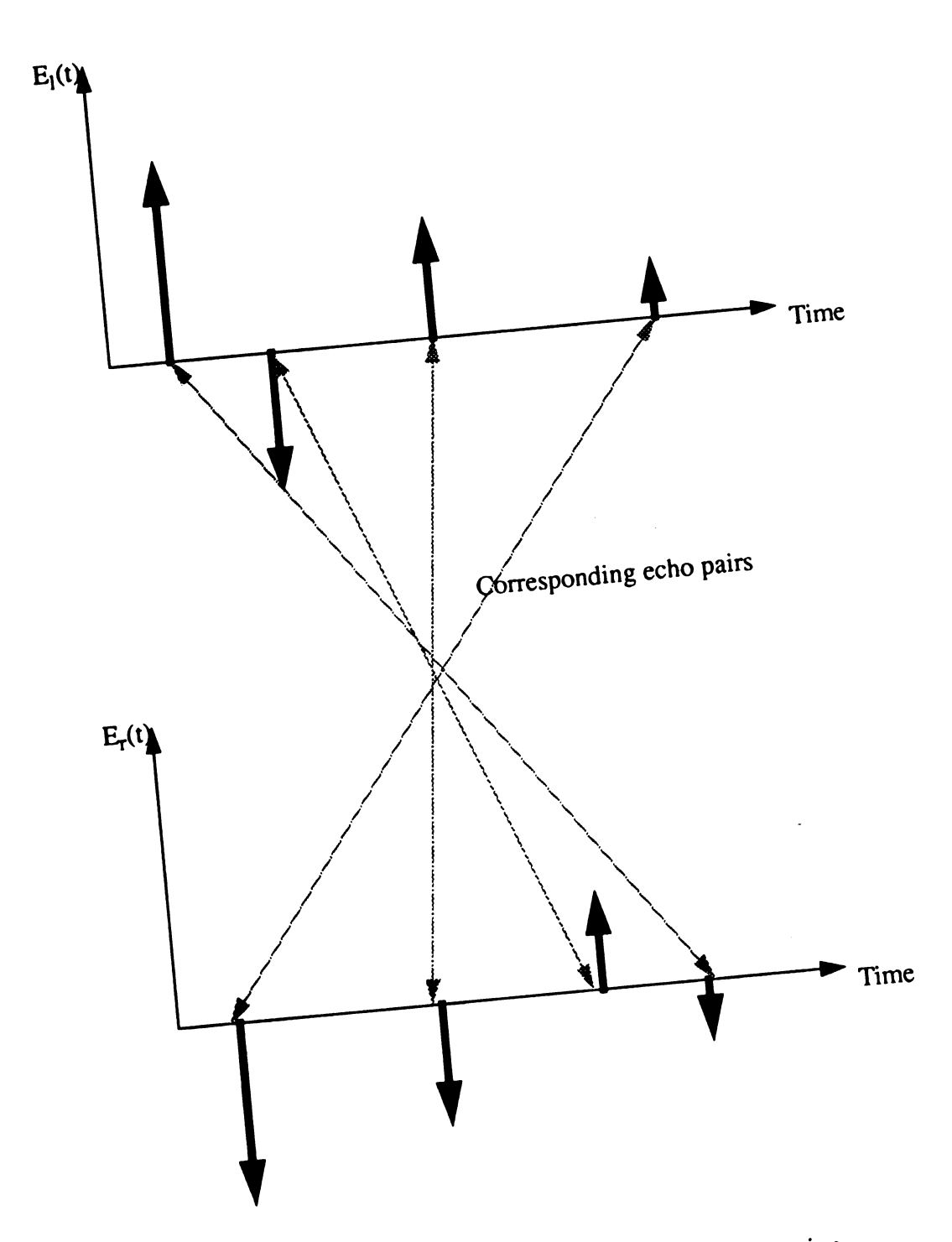


Figure 3.3. The impulse response pairs of dual interrogation.

Taking the ratio of two consecutive echoes received by the left transducer

$$\frac{E_{Li+1}(k,r)}{E_{Li}(k,r)} = k_i^2 \left(1 - r_i^2\right) \left(\frac{r_{i+1}}{r_i}\right) , \qquad (3.9)$$

the loss factor of layer i becomes

$$k_{i} = \left(\frac{E_{Li+1}(k,r)r_{i}}{E_{Li}(k,r)r_{i+1}\left(1-r_{i}^{2}\right)}\right)^{1/2}.$$
(3.10)

Similarly, this loss factor can also be obtained from the echo return received by the right transducer,

$$k_{i} = \left(\frac{E_{Ri}(k,r)r_{i+1}}{E_{Ri+1}(k,r)r_{i}\left(1-r_{i+1}^{2}\right)}\right)^{1/2} . \tag{3.11}$$

As a result, the loss factor of each layer can be expressed by the echo information from either side. The attenuation-velocity product of the layer i ca be expressed, from Eq.3.6, as

$$\alpha_i v_i = -ln(k_i) t_i^{-1} . \tag{3.12}$$

In reality, multiple reflections do exist in individual layer especially when the reflection coefficient at the interfaces are large. Under such a situation, it is impossible to solve the problem by using the equations given above. The multiple reflections of layer i is demonstrated in Figure 3.4. The echoes of layer i with infinite multiple reflections can be expressed as

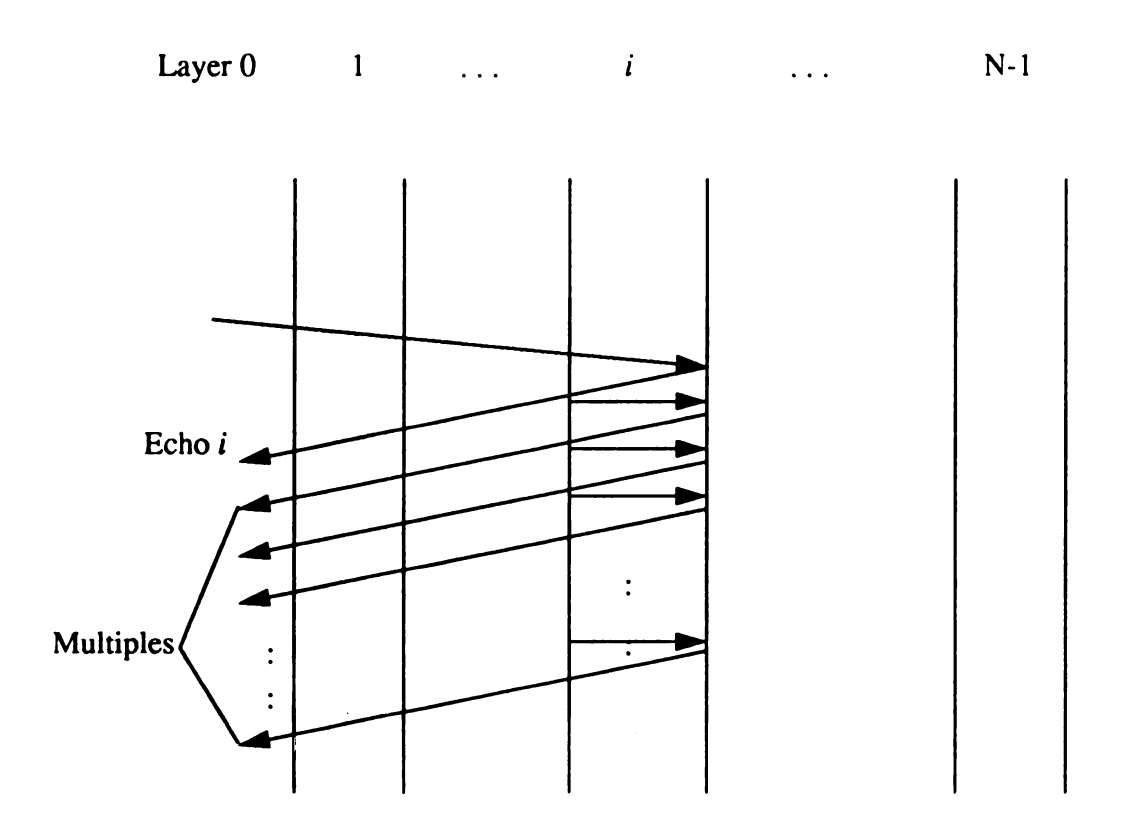


Figure 3.4. Multiple reflections of layer i.

$$E_{LMi}(k,r) = E_{Li}(k,r) \left[1 + \sum_{n=1}^{\infty} (-1)^n r_{i-1}^n r_i^n k_i^n \right]$$
 (3.13)

where n=1 to ∞ .

The multiple reflections of layer i is a train of echoes which are equally spaced in time. In order to eliminate multiple reflections, we utilized the properties of the primary echo of layer i:

a)
$$\operatorname{Time}(E_{Li}(k,r)) + \operatorname{Time}(E_{Ri}(k,r)) = \operatorname{Time}(T_{LR}(k,r)) + \operatorname{Time}(T_{RL}(k,r))$$

b)
$$\operatorname{Sign}(E_{Li}(k,r)) = -\operatorname{Sign}(E_{Ri}(k,r))$$

Assuming that there is no overlapping between the echoes and the multiple reflections, the primary data set $\{E_L(k,r), E_R(k,r), T_{LR}(k,r), T_{RL}(k,r)\}_{primary}$ can be obtained from experimental data set $\{E_L(k,r), E_R(k,r), T_{LR}(k,r), T_{RL}(k,r)\}_{experiment}$ by the following algorithm. The reflection coefficients and attenuation-velocity products of all layers can then be evaluated.

Algorithm:
$$\{E_{I}(k,r), E_{R}(k,r), T_{IR}(k,r), T_{RI}(k,r)\}_{experiment}$$

Step 1. Echo acquisition. Obtain the experimental data set $\{E_L(k,r), E_R(k,r), T_{LR}(k,r), T_{RL}(k,r)\}$ experiment

Step 2. For i = 1 to {maximum echo number between $E_L(k, r)$ and $E_R(k, r)$ }

$$If (Time(E_{Li}(k,r)) + Time(E_{Ri}(k,r)) = Time(T_{LR}(k,r)) + Time(T_{RL}(k,r))$$
 and

$$Sign(E_{L_i}(k,r)) = -Sign(E_{R_i}(k,r)),$$

then save
$$E_{Li}(k,r)$$
 and $E_{Ri}(k,r)$ into $\{E_L(k,r), E_R(k,r), T_{LR}(k,r), T_{RL}(k,r), T_{RL}(k,r),$

Step 3. If $\{E_L(k, r), E_R(k, r)\}$ not empty, go to Step 2.

Step 4. Compute reflection coefficient r_i and attenuation-velocity product $\alpha_i v_i$ from $\{E_I(k,r), E_R(k,r), T_{IR}(k,r), T_{RI}(k,r)\}_{primary}$

Case 2. Using only the reflected signals

If the target is thick and/or extremely lossy, there may not be appreciable signal transmitted. Under such situation, the attenuation-velocity product (αv) and reflection coefficient (r) can be obtained by using the reflected signals alone, provided the initial signal strengths I_{L0} and I_{R0} are predetermined quantities. Taking the ratio of the consecutive echo amplitudes from the left return, one has

$$\frac{E_{Li}(k,r)}{E_{Li+1}(k,r)} = \frac{r_i}{r_{i+1}(1-r_i^2)k_i^2} . \tag{3.14}$$

Similarly, for the right-side return, the ratio is

$$\frac{E_{Ri}(k,r)}{E_{Ri+1}(k,r)} = \frac{r_i \left(1 - r_{i+1}^2\right) k_i^2}{r_{i+1}}$$
(3.15)

Multiplying equations (3.14) and (3.15), it yields

$$\frac{E_{Li}(k,r)E_{Ri}(k,r)}{E_{Li+1}(k,r)E_{Ri+1}(k,r)} = \frac{r_i^2 \left(1 - r_{i+1}^2\right)}{r_{i+1}^2 \left(1 - r_i^2\right)}.$$
(3.16)

The left-hand side of Eq. 3.16 can be obtained from the echo amplitudes received by the transducers situated on both sides of the target. The right-hand side of Eq. 3.16, however, contains two undetermined quantities, the successive reflection coefficients r_i and r_{i+1} . In other words, if we know the reflection coefficient of the very first interface, we can then evaluate all reflection coefficients by Eq. 3.16. We have assumed the target is submerged in water, the first reflection coefficient is then

$$r_1 = \frac{E_{L1}(k, r)}{I_{L0}k_0^2} \tag{3.17}$$

Since water is almost lossless, especially in a very shallow path, the value k_0 is approximately equal to unity. The incident signal strength I_{L0} can be evaluated by observing the echo reflected from a simple water-air interface setup as shown in Fig. 3.5. Therefore, the reflection coefficient of the first interface can readily be determined. After all reflection coefficients are evaluated, the loss factor k_i and thus the attenuation-velocity product of all layers can be determined by Eqs. 3.11 and 3.12.

3.1.2 Advantages and limitations

The time domain technique described in the previous section provides a simple way to determine both the reflection coefficient and attenuation-velocity product at the same time. It also deal with the multiple reflections within layers which usually cause artifacts in the ultrasonic image system [76]. On the other hand, this technique requires

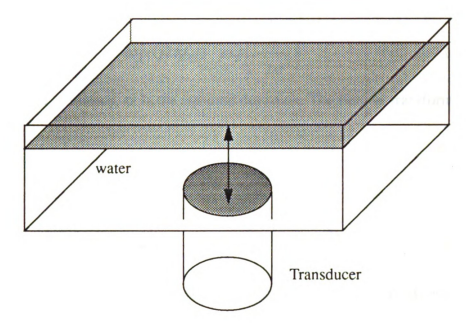


Figure 3.5. Experimental setup for incident signal measurement.

a good alignment of the transducer. A minor misalignment of the transducer with respect to the layer structure could cause a significant error at the end.

Assume that the incident acoustic signal has a Gaussian-shaped spectra:

$$x(t) = exp(j2\pi f_0 t) \cdot exp\left(-\frac{t^2}{2\sigma^2}\right)$$
 (3.18)

where f_0 is the central frequency, σ is the standard deviation. The Fourier transform pair of Eq. 3.18 will be

$$X(f) = \int_{-\infty}^{\infty} x(t) \cdot exp(-j2\pi ft) dt$$
$$= \sqrt{2\pi}\sigma \cdot exp\left[-2\pi^2\sigma^2(f-f_0)^2\right] . \tag{3.19}$$

The transfer function of the medium, when the attenuation factor is taken its account, has the following form

$$H(f) = exp(-\alpha f^{n}l) \cdot exp(-jkl)$$
 (3.20)

where αf^n is the attenuation factor, l is the travel distance. k is the wave number, and n is the frequency dependent factor (between 1 and 2). Then, the output spectrum will be

$$O(f) = X(f) \cdot H(f) = \sqrt{2\pi}\sigma \cdot exp\left(-2\pi^2\sigma^2(f - f_0)^2\right) \cdot exp\left(-\alpha lf^n\right) \cdot exp\left(-jkl\right) . \tag{3.21}$$

Most of the materials have a linear frequency dependency, i.e. n=1, the inverse Fourier transform becomes

$$o(t) = exp\left(-\alpha l f_0 + \frac{\alpha^2 l^2}{8\pi^2 \sigma^2}\right) \cdot exp\left(-\frac{\left(t - \frac{l}{\nu}\right)}{2\sigma^2}\right).$$

$$exp\left\{j2\pi\left(f_0 - \frac{\alpha l}{4\pi^2 \sigma^2}\right) \cdot \left(t - \frac{l}{\nu}\right)\right\} . \tag{3.22}$$

The maximum amplitude of o(t) occurs at t=l/v and the peak value is

$$o_p(t) = exp\left(-\alpha f_0 + \frac{\alpha^2 l^2}{8\pi^2 \sigma^2}\right)$$
 (3.23)

It can be concluded that the output is strongly dependent on the spectra of the incident signal as well as the exponential function of the attenuation coefficient. This method has following drawbacks:

- (1). Error accumulation. Since the incident signal of a given layer is the transmitted signal from the previous layer, whatever error contains in the signal will propagate on. The error is then accumulative.
- (2). The acoustic pulse is in general not a narrowband signal in the spectral domain.

 This will cause analytical error as described in Eq. 3.23.
- (3). Normal incidence of the signal is assumed. Error will be introduced otherwise.

3.2 Frequency domain technique

If a broadband signal can be implemented in the ultrasonic system, the attenuation property of the material can be estimated by observing the spectral distributions of the incident and reflected waves. Two methods are commonly used; the spectral difference [1,43,77] and the spectral shift methods [41,44,52,55]. The spectral difference method

estimates the attenuation factor from the difference of slopes between the low region and far region of the log spectra. The advantage of this method is that no specific spectral form of incident signal is required. The drawback is the frequency deference method didn't consider reflection and the attenuation as separate factors. On the contrary, the estimated attenuation factor also contain the reflection information. Thus, the estimation results are contaminated and the accuracy is not as good as the spectral shift method described next.

When an acoustic signal passes through a medium, there will be a down-shift effect of the central frequency in the spectra of the echo signal. This is due to the fact that higher frequency components of acoustic signal suffer higher attenuation than that of the lower ones. The spectral shift method estimates the attenuation and reflection coefficients from this down-shift information. Assume that the incident pulse has a Gaussian-shaped spectra as described in Eq. 3.18 and the transfer function of the media is characterized as:

$$H(f) = exp\left(-\alpha_i f^n l_i\right) \tag{3.24}$$

where α_i is the attenuation coefficient of layer i, n is the exponent of frequency dependent, l_i is the thickness of i-th layer.

The model of the multi-layered structure is shown in Figure 3.6. When there is a normal incidence, the amplitude of the received echo signals from each boundary can be expressed as:

$$|O_{i+1}(f)| = |X(f)| \cdot |R_{i+1}(r_1, ..., r_{i+1})| \cdot \prod_{k=1}^{i} |exp(-2\alpha_k l_k f^n)|^2$$
 (3.25)

where X(f) is defined as Eq. 3.19, and $R_{i+1}(r_1, ..., r_{i+1})$ is the reflection function and can be expressed as:

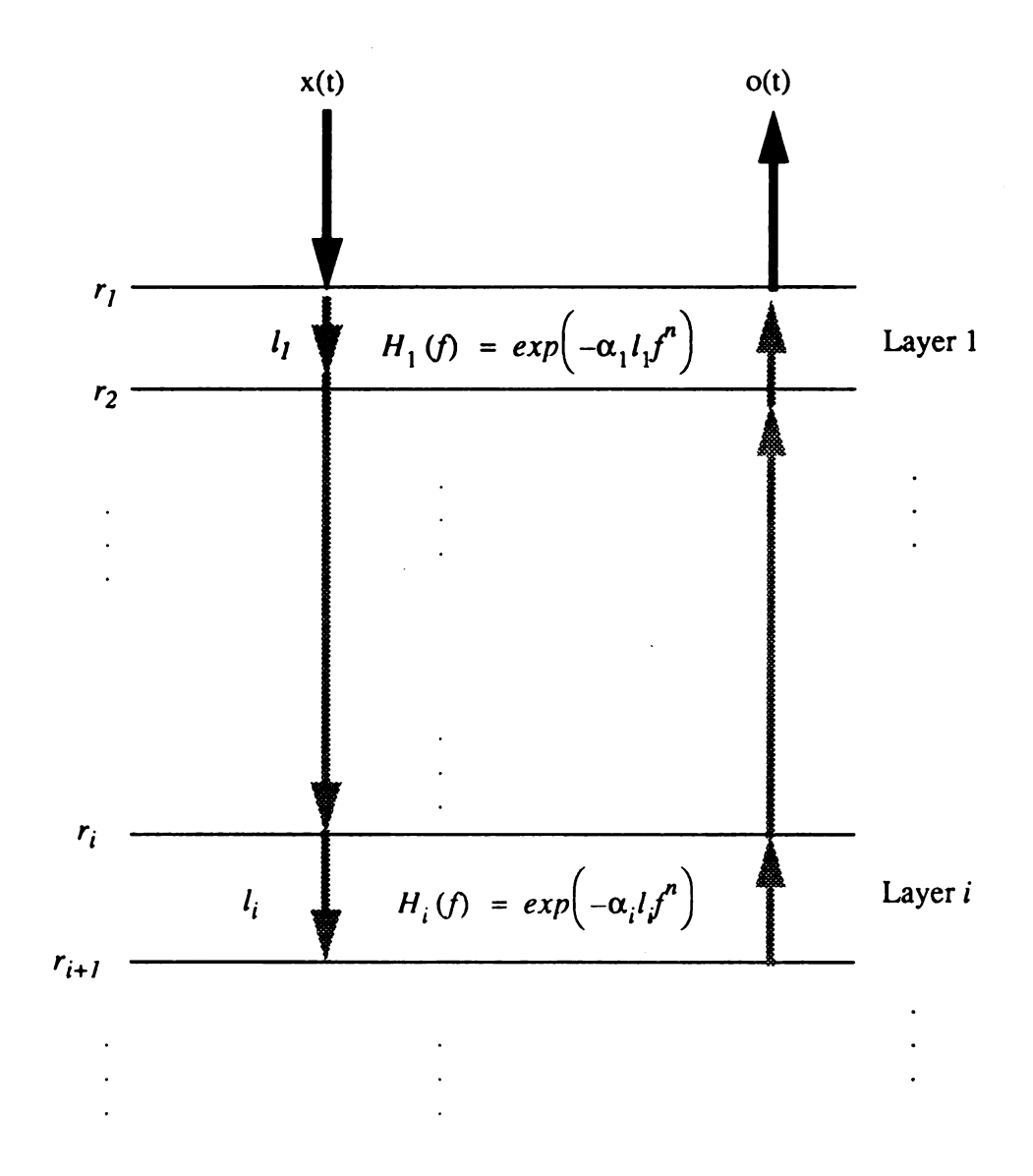


Figure 3.6. Structure of multi-layered model for frequency domain method.

$$R_{i+1}(r_1, ..., r_{i+1}) = r_{i+1} \prod_{k=1}^{i} \left(1 - r_k^2 \right)$$
 (3.26)

for i=1 to N.

Let us consider the linear frequency dependency case, i.e. n=1. The echo pulse spectra from the boundary (i+1)-th can be expressed as:

$$|O(f)| = K_{i+1} \cdot |R_{i+1}| \cdot exp(-2\pi^2 \sigma_0^2 (f - f_{i+1})^2)$$
 (3.27)

 K_{i+1} is a frequency-independent constant.

Assume that the first layer is water or couplant such that the attenuation is very small. Then, the central frequency of layer i+1 will be

$$f_{i+1} = f_0 - \frac{1}{2\pi^2 \sigma_{0k=1}^2} \sum_{k=1}^{i} \alpha_k l_k$$
 (3.28)

for i=1 to N.

From Eq. 3.25, the frequency difference of two successive layers will be:

$$\Delta f_i = f_{i+1} - f_i = \frac{1}{2\pi^2 \sigma_0^2} \alpha_i l_i \tag{3.29}$$

for i=1 to N.

So, the attenuation coefficient of *i-th* layer, α_i , can be obtained from Eq. 3.26 as

$$\alpha_i = \frac{2\pi^2 \sigma_0^2 \Delta f_i}{l_i} \quad . \tag{3.30}$$

Since l_i is usually unknown in a real situation, the product $\alpha_i l_i$ is the quantity to be used to estimated the attenuation property of materials. In order to obtain the reflection coefficient of each layer, let us look at the amplitude ratio of two successive echoes.

$$\frac{p_{i+1}}{p_i} = \frac{\left| X(f_{i+1}) \right| \cdot \left| R_{I+1} \right| \cdot \prod_{k=1}^{i} \left| H_k(f_{i+1}) \right|^2}{\left| X(f_i) \right| \cdot \left| R_I \right| \cdot \prod_{k=1}^{i-1} \left| H_k(f_i) \right|^2}$$

$$= \frac{\left|X\left(f_{i+1}\right)\right| \cdot \prod_{k=1}^{i} \left|H_{k}\left(f_{i+1}\right)\right|^{2}}{X\left(f_{i}\right) \cdot \prod_{k=1}^{i-1} \left|H_{k}\left(f_{i}\right)\right|^{2}} \cdot \left|\frac{r_{i+1}\left(1-r_{i}\right)^{2}}{r_{i}}\right|$$
(3.31)

for i=1 to N.

From the measured data, i.e., p_{i+1} and p_i , and the estimated attenuation coefficient of each layer obtained from Eq. 3. 30, the reflection coefficient of each layer can be obtained as

$$|r_{i+1}| = \frac{|r_i|}{(1-r_i)^2} \cdot \frac{p_{i+1}}{p_i} \cdot \frac{X(f_i) \cdot \prod_{k=1}^{i-1} |H_k(f_i)|^2}{|X(f_{i+1})| \cdot \prod_{k=1}^{i} |H_k(f_{i+1})|^2}$$
(3.32)

for i = 1 to N.

Ho et. al. [78] has developed extended work on nonlinear frequency-dependent case (1<n<2) in attenuation estimation.

Although the spectral shift method can provided both the reflection coefficient and attenuation-thickness product of each layer, it suffers from the following drawbacks:

- (1). The incident signal must assume to have the Gaussian-shaped spectra. This may not be the case in the real system.
- (2). The error is accumulative from layer to layer. That is, the error in the previous layer will propagate to the next layer and so on.
- (3). In the analysis given, the frequency dependent exponent, n, of each layer is assumed to be the same.
- (4). The incident signal is to be normal to the boundaries of the structures which is difficult to accomplish in experimental setup. This is also not true for real situation.
- (5). The multiple reflections within layer are ignored. This is may not be true for medium with low attenuation and large reflection coefficients.

Experimental setup and results of time domain technique on multi-layered model will be described and demonstrated on Chapter 5.

Chapter 4

4.0 Material Characterization Using Unsupervised Competitive Learning

In this chapter, a new methodology is proposed to resolve the material characterization problem quantitatively. First, the overall concept and background will be introduced. Then, details of each stage in the unsupervised learning will be given. Neural network for unsupervised learning is also included. Two clustering algorithms and two cluster validity indices are developed.

4.1 Introduction

The estimation and measurement of attenuation properties of biological tissues has received much attention in the field of ultrasonic tissue characterization. During the past two decades, many clinical studies and measurements on liver, breast, and myocardial tissues demonstrated correlations between pathological status and tissue attenuation values [9,41,42,79,80]. In spite of the encouraging results showing that attenuation measurement of biological tissues may provide a useful noninvasive tools for diagnosis, tissue attenuation measurement or estimation in vivo applications is still a very difficult and

tedious task [81,82]. Difficulties arise from the facts that the acoustic wave is scattered by the biological structures and that the media are dispersive in nature. Although some improvement can be made in data acquisition techniques, nevertheless, tissue characterization based on the information from scattered ultrasonic signal is by no mean trivial since itself is a random process [2,18].

Methods for attenuation estimation can generally be divided into two categories. The time-domain method [46,55,82] has the advantage of being easily implemented and thus is suitable for real-time processing. However, it can only provide limit amount of information. On the other hand, the frequency-domain methods [1,83,84] give more feature parameters and better accuracy. The trade-off is that it requires more extensive processing procedures such as windowing and FFT, those will introduce new variance into the estimation values.

Material characterization utilizes its estimated attenuation property is not reliable at the present time. In order to improve the accuracy of identification, we proposed a method of applying the clustering technique based on the features extracted from the echo return signals. The competitive unsupervised learning technique using layered artificial neural network structure is used to classify the multi-dimensional data set into clusters after features are extracted from the returns. Image processing technique will be used for adding spatial information to the clustering result. This method can be applied to both the conventional B-scan and C-scan imaging reconstructions. The advantages of the proposed method are outlined below.

- (1). Since many features are to be used for material characterization, both time-domain and frequency-domain information will be utilized.
- (2). Features can easily be added or deleted from the feature space for the improvement of classification capability.

(3). Does not require the knowledge of the frequency spectrum of the incident acoustic pulse which is very difficult to obtain experimentally or the relationship between attenuation coefficient and frequency.

The presentation is organized as follows. The feature extraction section describes how the features are extracted from the pulsed-echo signals, and the procedure of selecting the independent features from the feature space. Next, competitive unsupervised learning technique which is implemented by artificial neural network is described. Clustering validity and local minimum problem will also be addressed. Finally, experimental setup and the segmented C-scan images using clustering information will be presented for various test objects. The system diagram is shown in Figure 4.1 and the unsupervised learning is composed of stages as shown in Figure 4.2.

4.2 Theoretical Background

From chapter 2, we know that the stress wave propagating in the x direction can be expressed as

$$p = p(0)\cos(2\pi f t - kx)$$
 (4.1)

where p is the pressure, p(0) is the maximum pressure, f is the frequency, and k is the wave number or reciprocal wavelength. As the pressure wave travels through a medium, it will experience a exponential decay in the amplitude with a factor $e^{-\alpha_f x}$, where α_f is the attenuation coefficient at frequency f and x is the distance the wave has traveled. Including the attenuation factor, the pressure variation becomes

$$p = p(0) e^{-\alpha_{f} x} \cos(2\pi f t - kx)$$
 (4.2)

In a real system, a transducer which is excited by a trigger pulse will produce a band of frequency components. Therefore, the total stress wave propagates through medium

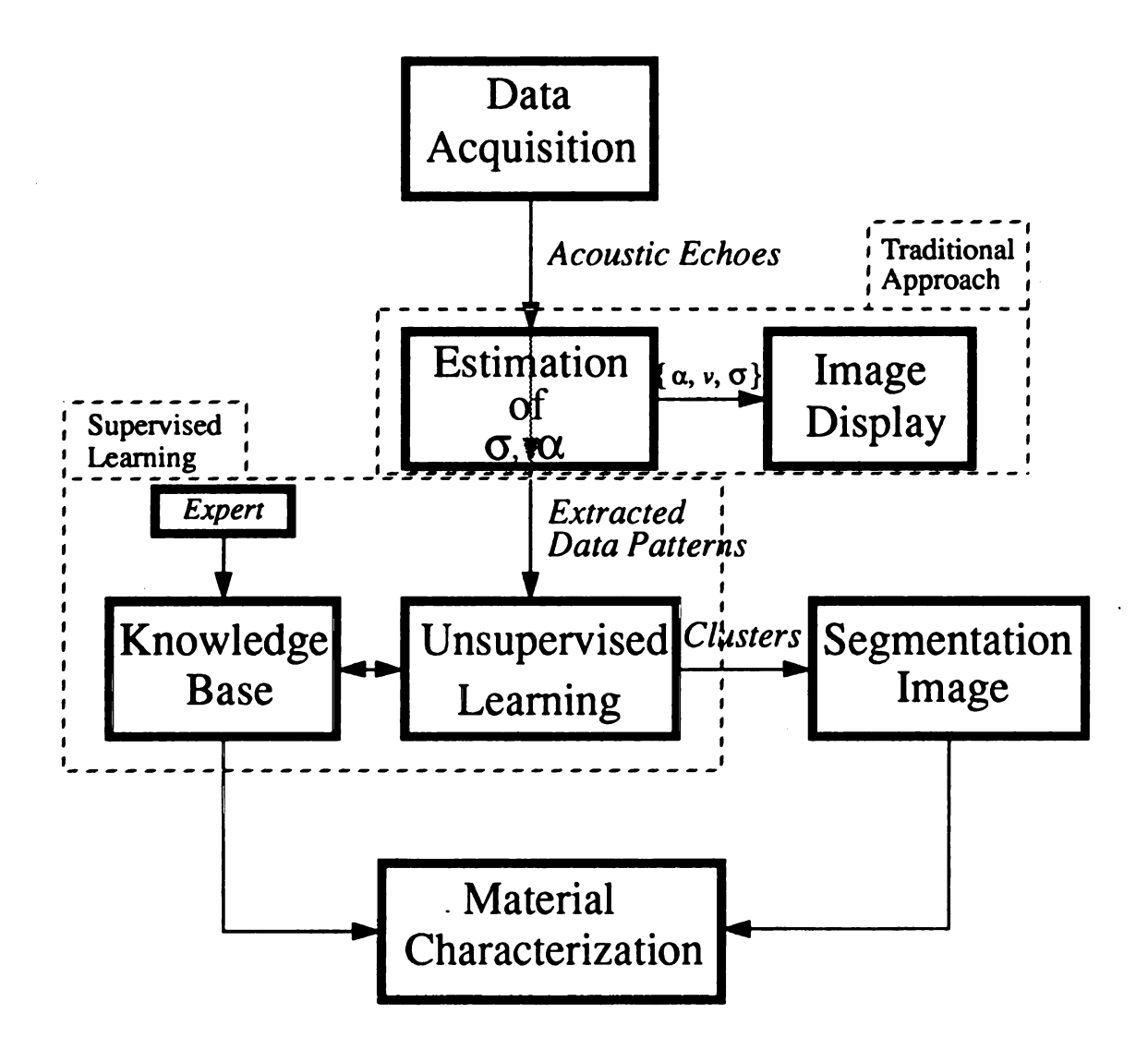


Figure 4.1. System diagram.

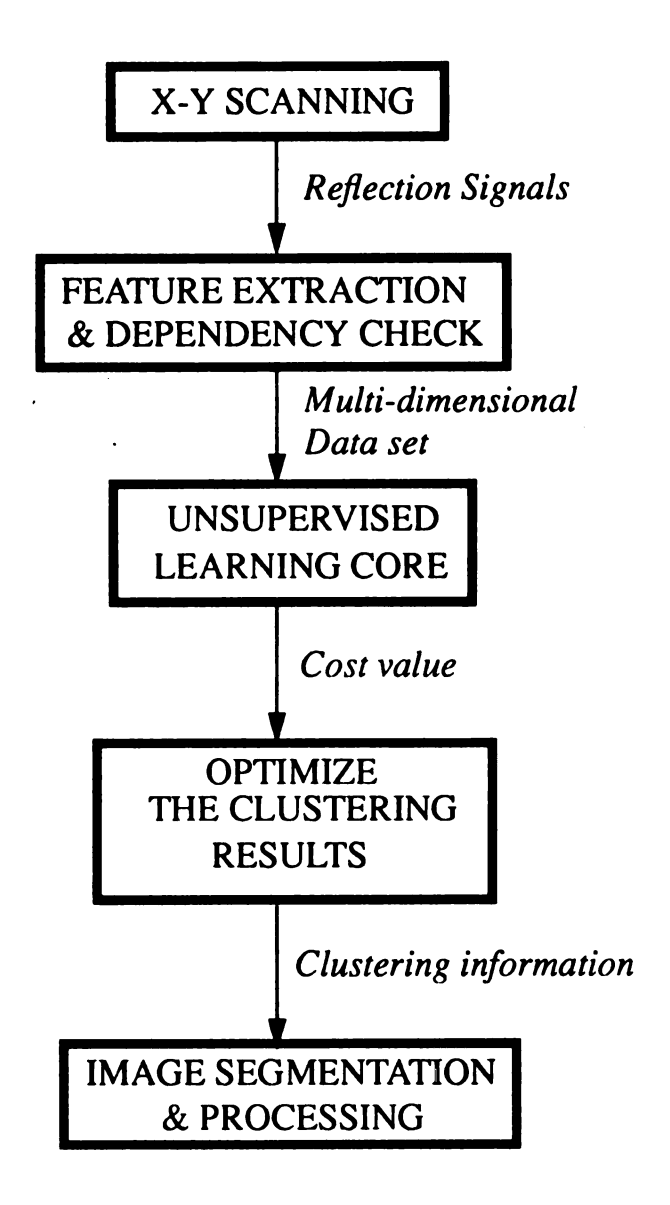


Figure 4.2. Stages of unsupervised learning.

becomes an additive effect of all frequency components and can be expressed as

$$P = P(f_1) e^{-\alpha_{f_1} x} \cos(2\pi f_1 - k_1 x) + P(f_2) e^{-\alpha_{f_2} x} \cos(2\pi f_2 - k_2 x) + \dots$$

$$= \sum_{i} p(f_i) e^{-\alpha_{f_i}} \cos(2\pi f_i - k_i x)$$
 (4.3)

where p(f) is the amplitude of excitation at the given frequency. If the material is dispersive, each component of Eq. 4.3 will travel with its own phase velocity $c_n = f_n/k_n$. Since the higher frequency components will be attenuated more than the lower ones, there will be a downshift of spectrum shape in the frequency domain.

Based on this principle, the attenuation coefficient of materials have been evaluated by several researchers, Dines and Kak [2], J. Ophir et al. [51], and Shaffer et al. [68]. However, either a known spectral shape of incident wave or n value has to be assumed

4.3 Feature Extraction

Five different features are extracted from each reflected signal at the initial phase of the process. That is, at each scanning position, five frequency-dependent features are extracted from each echo return. These features are: total energy, central frequency, peak frequency, 3-dB bandwidth of echo spectrum, and correlation coefficient between incident and reflected signals.

Total energy

The total energy of the reflected signal is related to the reflection coefficient, which contains the information of acoustic impedance of the medium. Let the sampled echo be s(N), then the total energy can be expressed as

$$E_{t} = \sum_{i=1}^{N} |s(i)|^{2}$$
 (4.4)

where N is the number of sampling points of each echo signal.

Central frequency, peak frequency, and bandwidth

Attenuation coefficient has been shown to be highly related to spectral-shift and spectral-difference of the echo spectrum [43]. These phenomena will cause central frequency and peak frequency shifted downward and in the meantime the 3-dB bandwidth of the echo spectrum will also be widened. For a Gaussian-shaped spectrum, the center frequency can be estimated by the mean frequency [85, 86], \overline{F}_m , and is given by

$$F_{m} = \frac{\sum_{i=1}^{N} F_{i} P(F_{i})}{\sum_{i=1}^{N} P(F_{i})}$$
(4.5)

where $P(F_i)$ is the *i-th* element of the N-point FFT, which is ranging from the lower 3-dB to the upper 3-dB level. The peak frequency PK(F) is the frequency having a maximum magnitude within the 3-dB bandwidth. Figure 4.3. shows these features on spectrum of echo signal.

Correlation between incident and reflected signals

Correlation between the reflected and incident signals at a given interface can provide useful information about the medium under interrogation. The properties such as elasticity, stiffness, velocity, and attenuation are all embedded in this feature.

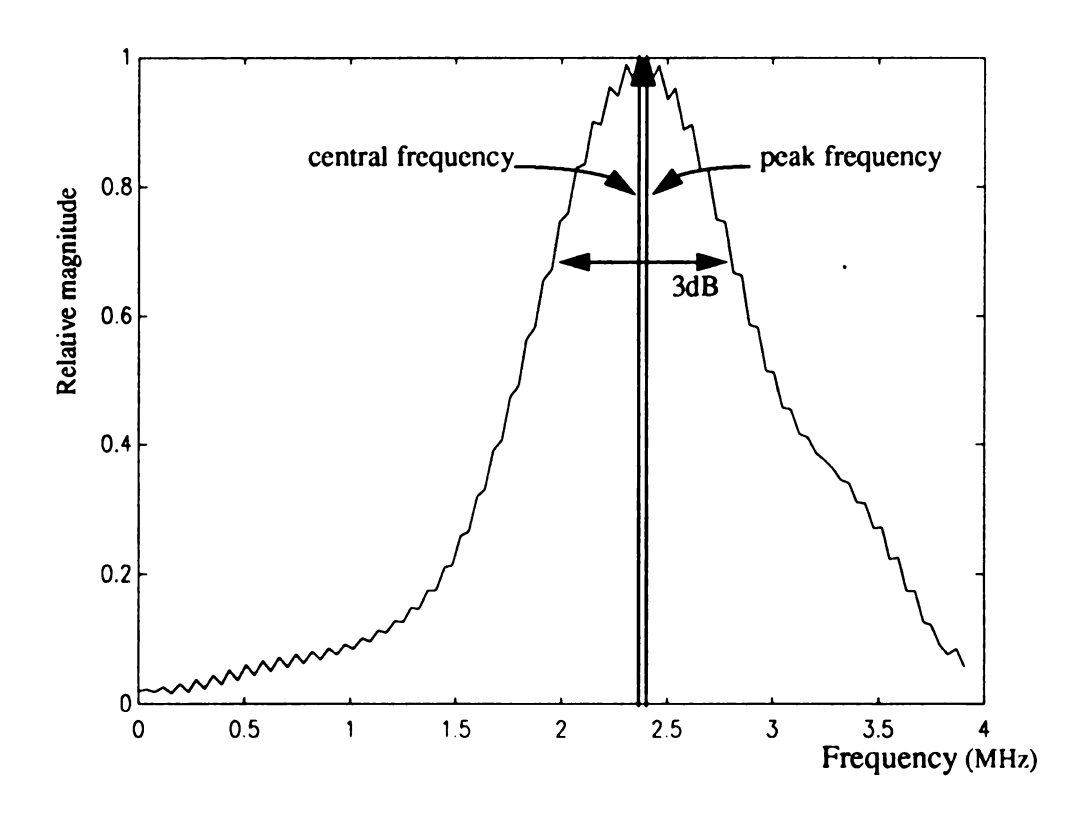


Figure 4. The three features in spectrum of echo signal.

In order to avoid redundant selection of the features, linear dependent test is performed to measure the degree of feature dependence between features. The linear dependency between two features, i and j, is measured by [87]

$$d(i,j) = \frac{\left(\frac{l}{n}\right) \sum_{r=1}^{n} (x_{ri} - m_i) (x_{rj} - m_j)}{s_i s_j}$$
(4.6)

where s_j and m_j are the sample variance and sample mean, respectively, for feature j respectively. The absolute value is used since the correlation could have either a positive or negative value. The magnitude is being used as an index for dependency. If d(i,j) = 0, the features i and j are linearly independent. Whenever d(i,j) approaches unity, one of the features can then be discarded.

4.4 Competitive unsupervised learning using neural networks

In this section, two unsupervised learning algorithms will be introduced and implemented with competitive neural network. The basic problem of competitive learning neural network will stated first. Followed by the comparison of convergence between different neural network models for unsupervised learning.

As described in chapter 2, the competitive learning network is the simplest way and the fastest way to perform the unsupervised learning. Yet, it suffers the dead units problem which make it less competitive when compared with other methods. The dead units problem can be prevented by the following ways:

(1). Update the weights of all the losers as well as the winner, but with a much smaller learning rate for the losers. This will make the units that never win gradually move towards the average of input patterns and eventually win the competition. The is

called leaky learning.

- (2). Update not only the weights of winner but also weights of its neighbors. This is basically the essence of Kohonen feature map and is discussed later.
- (3). Suppress the frequent winner by adding a frequency counter in the decision of winner. The frequent winner will become less competitive as it win more and give units that never win a increasing chance to win. This mechanism is sometimes called **conscience** method.
- (4). The input pattern vectors are smeared with additional noise, using a distribution with a long tail so that there is some positive probability for any input pattern [96].

Although the methods described above can avoid the dead units problem, they all pay the price on the computation load. A modified algorithm MFSCL will show improvement in computation load but also prevent the dead units problem in the later section.

Among the features of neural networks, learning ability is the most attractive one which makes it suitable for problems requiring large amount of computation and combinatorics. Pattern recognition belongs to this category of problems. Pattern recognition covers two types of learning: supervised and unsupervised learning [90]. In supervised learning, the learning is improved by the available class information of data patterns. On the other hand, unsupervised learning does not involve class information.

Among the models of neural networks for unsupervised learning, competitive learning [91] and Kohonen self-organizing feature maps [73] are the most widely used models in many applications. The self-organizing map basically involves competitive learning. During the training, connection weights of the winning neuron and its neighbors are updated. As training progresses, the size of neighborhood is minimized. As soon as the neighborhood size is reduced to one, the competitive learning is assumed to converge.

we begins with the basic competitive learning in this section. We then compare various

training algorithms for unsupervised learning, including the proposed training algorithm. Then, test data sets are used to justify our method. Finally, acoustic imaging segmentation results will also be presented.

4.4.1 Training Algorithms

A. Competitive Learning Neural Networks (CL): Let $X = \{x_d^{(1)}, ..., x_d^{(l)}\}$ be the training pattern vectors set, where the dimension of vectors is d. The class information of each pattern vector is unknown. The objective is to estimate the number of classes (clusters) for the given data set X. The output of each neuron in competitive learning is determined by

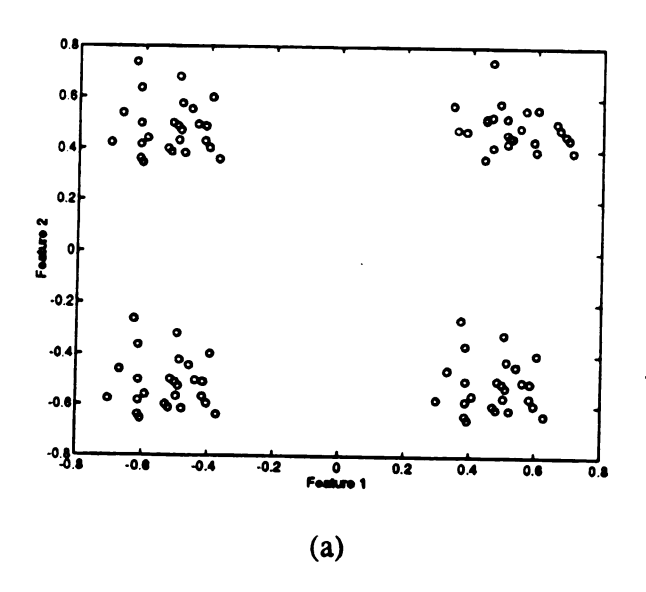
$$O_{i} = \begin{cases} 1 & \text{if } dist(x, W_{i}(n)) \leq dist(x, W_{j}(n)) \text{ for all } j \\ 0 & , Otherwise \end{cases}$$
(4.7)

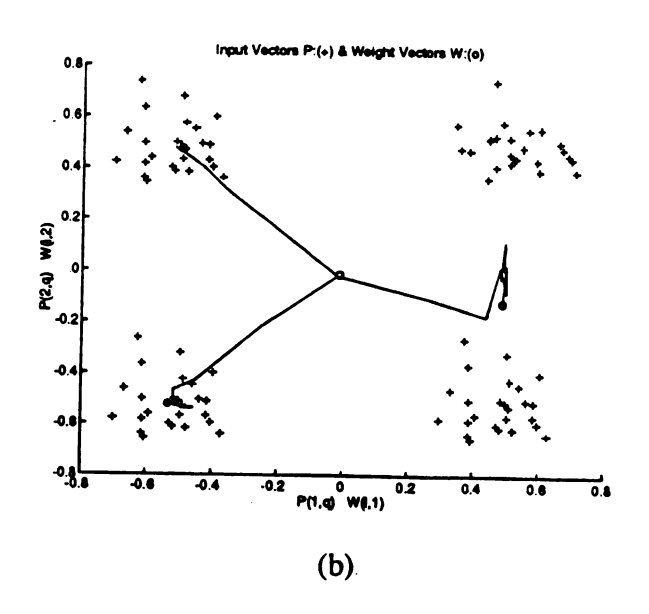
The dist(x,W(n)) is the Euclidean distance between vector x and the weight vector W(n). The weight updating rule of the neuron i is

$$W_{i}(n+1) = W_{i}(n) + \eta (x - W_{i}(n)) O_{i}$$
 (4.8)

where parameter η is the learning rate, and is typically decreased monotonically to zero as learning progresses.

The problem of competitive learning networks, according to its learning mechanism, is that it sometimes leads to unused neuron units, or the so-called *dead units* (underutilization) problem. That is, the network is trapped in a local minima for some initial weight vectors. Consequently, only some of the neurons get updated. The results on a two-feature data set with four clusters are used to demonstrated this problem. The initial weight





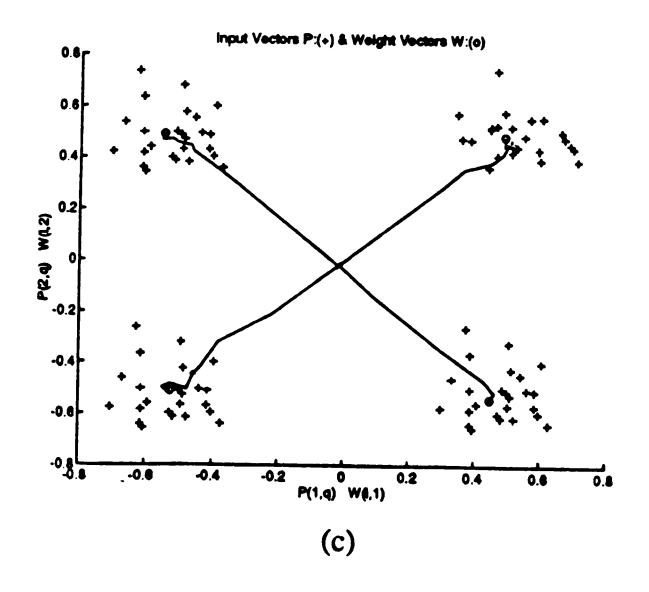


Figure 4.4. Demonstration of dead units problem. (a). A two-feature four clusters data set. (b). Result with a dead unit. (c). Result of MFSCL algorithm.

vectors of all the neurons were set close to the mean value of data set (-0.0103, -0.0160). As shown in Figs. 4.4(a) and 4.4(b), weight vector of one of the neurons was not updated during the training process. This problem was first discussed by Grossberg [92]. Later, Desieno [93] suggested conscience method to cope with this problem. However, conscience method is suitable for dividing data vector space into equiprobable regions. Unlike vector quantization, clustering needs different methods to yield the desirable result. This is because the clusters in a data set may contain different number of data patterns.

B. Kohonen Self-organizing Feature Maps (KSFM). The KSFM networks [73] and the competitive learning networks are similar in weight updating rule. However, in the KSFM structure each neural unit has its topological neighborhood. During the training process, the weight vectors of winning neuron as well as the weight vectors of its topological neighbors are all updated. The size of the neighborhood is decreased during the training progresses until the neighborhood

size equals to one. As a result, KSFM will become competitive learning network after a certain epochs of training. The weight updating rule of neuron *i* and its neighborhood will be

$$W_{i}(n+1) = \begin{cases} W_{i}(n) + \eta [x - W_{i}(n)], i \in N(i^{*}) \\ W_{i}(n), Otherwise \end{cases}$$
(4.9)

where $N(i^*)$ is the topological neighbors of neuron i. Again, the learning rate η decreased as training progresses.

Because of the weight vectors of both winning neuron and its neighbors are updated, the KSFM structure indeed avoids the dead units problem. However, it pays a high price of additional computation load as compared to the competitive learning. This computation load is coming from the weight vectors calculation and updating for the neighbors and

winning neuron itself. We suggest an alternative network that reduces the additional computation load and in the meantime resolve the dead unit problem.

C. Modified frequency-sensitive competitive learning (MFSCL). The motivation of the modified frequency-sensitive competitive learning is to overcome the limitations of simple competitive learning network while retaining its computational advantages. From our experience, dead units occur either at the beginning of the training phase or when weight vectors are trapped in pool mean of clusters during the training. In other words, some neurons could never be activated from the beginning of training because of the corresponding weight vectors are too far away from the input patterns in the pattern space. The KSFM uses multiple activation of neurons to avoid this trap. The frequency-sensitive competitive learning (FSCL)[95] introduces the winning frequency of each neuron to the distance calculation for the next winner. This method ensures that all neurons have equal opportunity and approximately equal number of times to be modified for avoiding dead units problem.

In FSCL network, each neuron incorporates a count of the number of times it has been the winner. Also, the distance measure to determine the winner is modified as

$$dist^*(x, W_i) = dist(x, W_i) \varphi_i(n)$$
 (4.10)

where $dist(x,W_i)$ is the Euclidean distance between x and W_i as described previously. $\varphi_i(n)$ is the count of winning frequency of neuron i during the training. If a given neuron wins the competition frequently, the count and the dist will increase as well. This reduces the likelihood that this neuron will again be a winner, and give other neurons with lower frequency count a higher chance to win the competition. Consequently, only the weight vector of the winning neuron is updated by Eq. 4.8.

The FSCL networks do achieve the goals of avoiding dead units problem and reducing computation load as compared to KSFM. However, it presents two drawbacks. First,

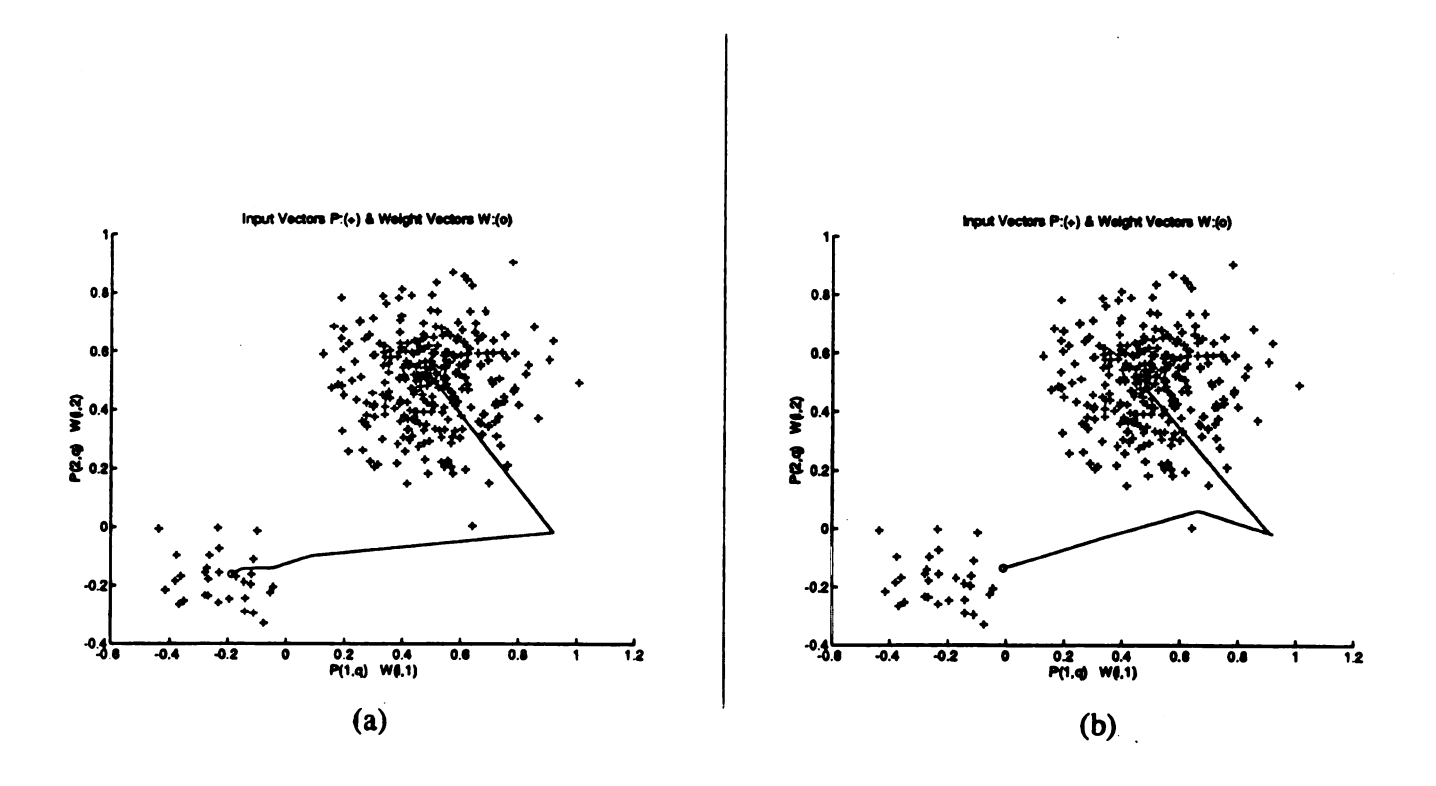


Figure 4.5. Comparison of clustering results when size of clusters are different with same initial weight vectors, training sequence and learning rate. (a). Results of MFSCL method. (b). Results of FSCL methods.

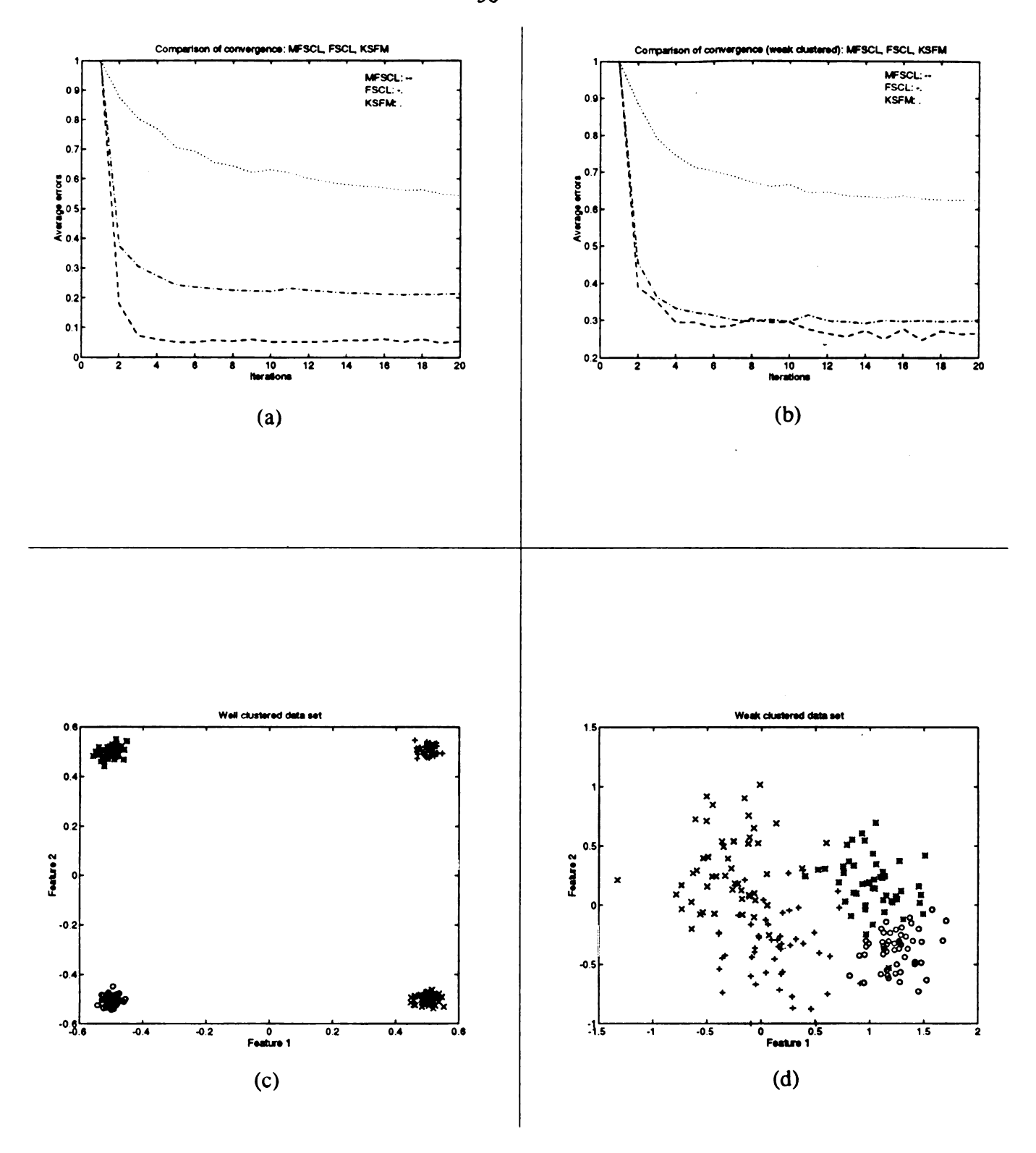


Figure 4.6. (a). Convergence comparison between MFSCL, FSCL, and KSFM methods using well clustered data set. (b). Convergence comparison between MFSCL, FSCL, and KSFM methods using weak clustered data set. (c). Display of well clustered data set. (d). Display of weak clustered data set.

pattern data set tends to be partitioned into same size of clusters as training progresses. Second, for data pattern set contains various size of clusters, the clustering results, i.e. cluster centroids, will be less optimal compared to other methods. This phenomena is demonstrated in Figure 4.5 by using same initial weight vectors and training sequence for FSCL and MFSCL methods.

Unlike the FSCL algorithm which uses frequency information during the entire training process, we introduce an algorithm that employes the frequency information only at the beginning of the training process and at situation when average error (distance) reaches minima. After sensing all neurons have been modified, the learning follows the CL mechanism. Therefore, the MFSCL method not only avoid dead units but also provides better clustering results than FSCL on data sets with various size of clusters. Using the same data set as in Fig. 4.4(a) the dead units problem is resolved by MFSCL and the result is shown in Fig. 4.4(c). Furthermore, it requires less computation time than FSCL and KSFM methods. A comparison of convergence of KSFM, FSCL, and MFSCL with same initial weight vectors and same presentation sequence on weak clustered data set and well clustered data set are shown in Fig. 4.6. The algorithm of MFSCL is described below.

Algorithm: Modified Frequency-Sensitive Competitive Learning (MFSCL)

Step 1: Set C=1.

Step 2: Initialize weight vectors and set all frequency counters of output neurons to zero.

Step 3: Choose the input pattern randomly and if all neurons have been updated set C equal to zero.

Step 4: Present the pattern to the networks

Determine the winner by Eq. 4.10 if C equal to one, else by Eq.

4.7.

Update the weight vector of winning neuron, and its frequency counter if C equal to one.

- Step 5: If $\Delta E^2 \le \varepsilon$, then go to Step 6, else go to Step 3.
- Step 6: Perturb the results by presenting all patterns once by Eq.4.10.

If new results better than that of Step 5, then go to Step 3.

Else stop and done.

The ΔE^2 is the average error (distance) between two consecutive epochs and ϵ is the threshold value for stopping the learning.

4.4.1.1 Cluster Validity

After the clustering process is performed, the next task is to find the most suitable number of clusters for the given data set. This problem continues to evade solution in cluster analysis. To circumvent this problem, many indices are evaluated by Milligan and Cooper [95]. Here, we adopted an internal index, the modified Hubert's (MH) Gamma, suggested by Jain and Dubes[87] because of its best performance. This statistic is the point serial correlation coefficient between proximity matrix of data patterns and a model matrix. In order to obtain the model matrix, distance between two patterns is set by the distance between centers of two clusters to which the patterns belong. The MH index is defined as following.

Let L denote the label function that maps the sets of patterns to the set of cluster labels and expressed as:

$$L(i) = k \quad \text{if } i \in C_k \tag{4.11}$$

Parameters that defined the average distance between all patterns, average distance between clusters, and two standard deviation are defined as:

$$r = \left(\frac{1}{M}\right) \sum \sum \delta\left(\underline{X}_{i}, \underline{X}_{j}\right) \delta\left(\underline{m}_{L(i)}, \underline{m}_{L(j)}\right) \tag{4.12}$$

$$M_{p} = \left(\frac{1}{M}\right) \sum \sum \delta(X_{i}, X_{j}) \tag{4.13}$$

$$M_{c} = \left(\frac{1}{M}\right) \sum \sum \delta\left(\underline{m}_{L(i)}, \underline{m}_{L(j)}\right) \tag{4.14}$$

$$\sigma_P^2 = \left(\frac{1}{M}\right) \sum \sum \delta^2 \left(\underline{X}_i, \underline{X}_j\right) - M_p^2 \tag{4.15}$$

$$\sigma_C^2 = \left(\frac{1}{M}\right) \sum \sum \delta^2 \left(\underline{m}_{L(i)}, \underline{m}_{L(j)}\right) - M_c^2 \tag{4.16}$$

where $M=n^*(n-1)/2$, $\delta(x, y)$ is the Euclidean distance between x and y, X is the pattern vector, $\underline{m}_{L(i)}$ is the mean vector of cluster i. Using the parameters defined above, the MH index for the clustering $\{C_1, \ldots, C_K\}$ is expressed as:

$$MH(K) = \frac{r - M_p M_c}{\sigma_P \sigma_C} . (4.17)$$

The number of clusters is estimated by seeking a significant knee in the MH versus number of clusters plot. Although there is no theoretical proof, MH index will decrease if true clusters were forced to merge or split. But if data set is grouped into more clusters than that of the data set itself, the MH index will be increased because of good correlation between data patterns. The MH statistic is bounded between 0 and 1.

4.4.2 Modified K-means (MK) algorithm using competitive learning

The second algorithm for the competitive learning is basically modified from the K-means method [88] and implemented by ANN structure. The algorithm is described as follows.

MK Algorithm: Data pattern set: {X}.

- Step 1. Randomly select data patterns as the cluster centroids (C_i) from data pattern set $\{X\}$.
- Step 2. Assign data pattern to the nearest cluster and modified the very cluster centroid until all data patterns are presented.
- Step 3. Reassign each data pattern to the cluster with nearest distance.
- Step 4. If classification of all data patterns remain unchanged,

perturb the clustering results.

If the results unchanged, then stop.

Else go to step 2.

Else go to step 2.

In step 4, the perturbation includes two procedures for escaping from the local minima.

First, different presentation order of data patterns are presented to the unsupervised learning mechanism. Second, shuffle boundary data patterns to different clusters. The clustering result with K clusters is determined by the cost function $S=S_w/S_b$. The with-class-scatter, S_w , is defined as

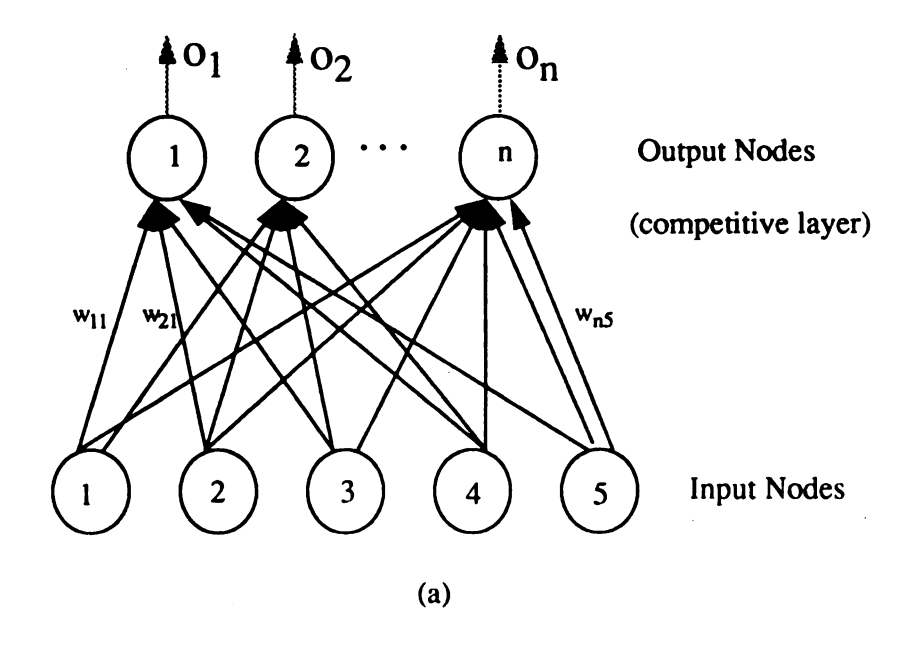
$$S_{w} = \sum_{k=1}^{K} \sum_{j=1}^{n_{k}} \left(x_{j}^{k} - m^{k} \right) \left(x_{j}^{k} - m^{k} \right)^{T}$$
(4.18)

where K is the number of clusters, n_k is the number of patterns in the k-th cluster, x_j^k is the pattern vector belong to the k-th cluster, and m^k is the vector feature means of the k-th cluster. The between-class-scatter, S_b , is defined as

$$S_b = \sum_{k=1}^K \sum_{j=1}^{n_k} {n \choose m^k - m} {m^k - m}^T$$
 (4.19)

where the pooled mean, m, is the grand mean vector for all patterns.

The smaller the S_w , the more compactness will be the cluster. A larger value of S_b implies the cluster is more isolated. Following the modified K-means clustering algorithm, the clustering results are determined by the cost function $S = S_w/S_b$. As a result, a small cost value of the cost function



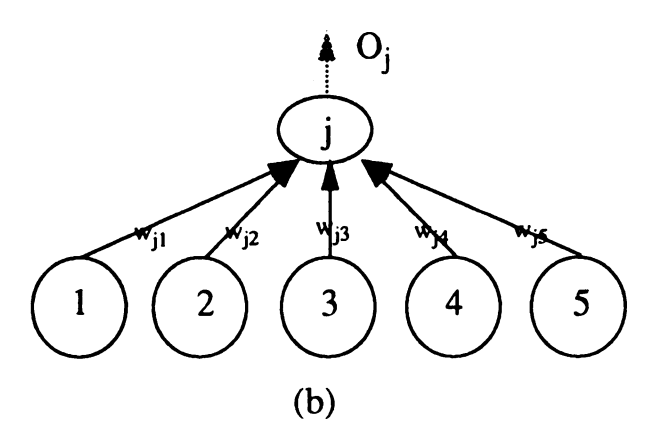


Figure 4.7 (a). Configuration of competitive neural network with n clusters and five features. (b) Function of sigle neuron.

will give a better clustering result.

Because of correspondence of the procedure, the unsupervised competitive neural network, as shown in Figure 4.7(a), was chosen to implement the algorithm. The number of input nodes represents the dimensionality of the input patterns, while the number of output nodes represents the

number of clusters. The function of each neuron is shown in Figure 4.7(b). Each time when a pattern is presented, only one of the neurons will be activated and gives an output of unity. This is accomplished by the following steps [89]: When the pattern vector X_i is presented to the network, the weight values of every neurons are computed by

$$S_i = \sum_{d=1}^{D} X_i W_{id} \qquad \text{for all } i.$$
 (4.20)

The output of neuron j, O_j , will be forced to 'one' when S_j is larger than S_k , for all k. D is the dimensionality of input pattern. Only the weighting vector (centroid) of neuron j (cluster j) is updated by

$$\Delta w_{ji} = l \left(\frac{X_i}{m} - w_{ji} \right) \tag{4.21}$$

$$w_{ji}^{new} = w_{ji}^{old} + \Delta w_{ji}$$
 (4.22)

where l is the learning rate and m is a normalization factor.

4.4.2.1 Cluster Validity

After the clustering is performed, the next task is to find the optimal number of clusters for the given data set. This remains an unsolved problem in cluster analysis, However, a heuristic method can be adopted to give the best estimation. If the clusters are meaningful, the cost value will decrease dramatically as the number of clusters increases. Therefore, the last knee point in the cost value versus the number of clusters plot is used to determine the number of clusters for a given data set. Figure 4.8 shows the knee point in the cost value curve.

A detail comparison between the above two algorithms will be given in Chapter 5 using Monte Carlo analysis on different data sets.

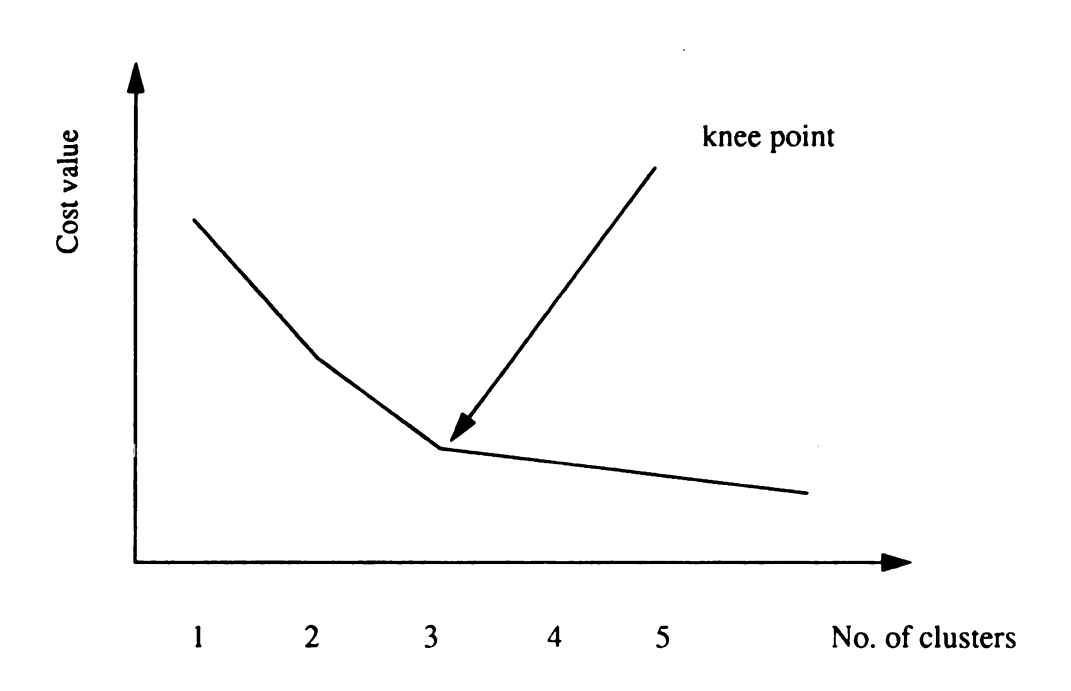


Figure 4. Cost value v.s. number of clusters.

Chapter 5

5.0 Simulation and Experimental results

In this chapter, experimental results were given to demonstrate the theoretical derivations of time domain technique. In the second section, a Monte Carlo method will be used to study the algorithms and indices discussed in the previous chapter using synthetic data sets. Finally, the results of material characterization using unsupervised learning method will be given and discussed.

5.1 Experimental results of time domain technique

In order to justify the theory described in chapter 3, two cases of experiments were conducted under the experimental setup as shown in Figure 5.1. The experimental setup includes a PC-486, a PC-based A/D converter board with 40 MHz sampling rate and 8-bit resolution (WAAG II), a Panametrics Inc. 5050 PR pulser, and two Panametrics V306 transducers. The central frequency of transducers is 2.25 MHz and their diameter is half inch.

In the first case, two single layer materials, plexiglass and aluminum, were used in the experiment separately to test the feasibility of experimental setup and observed errors

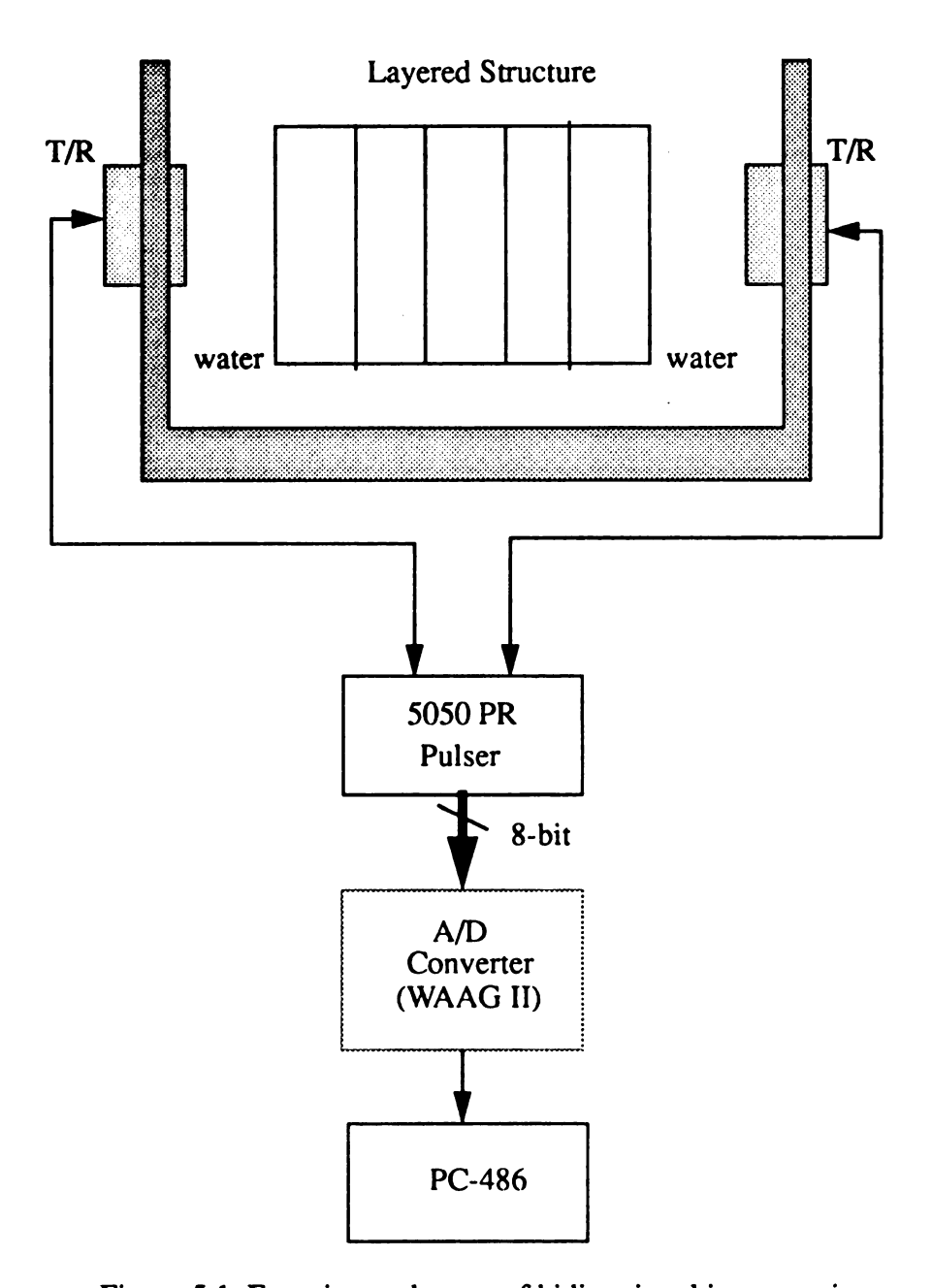


Figure 5.1. Experimental setup of bidirectional interrogation.

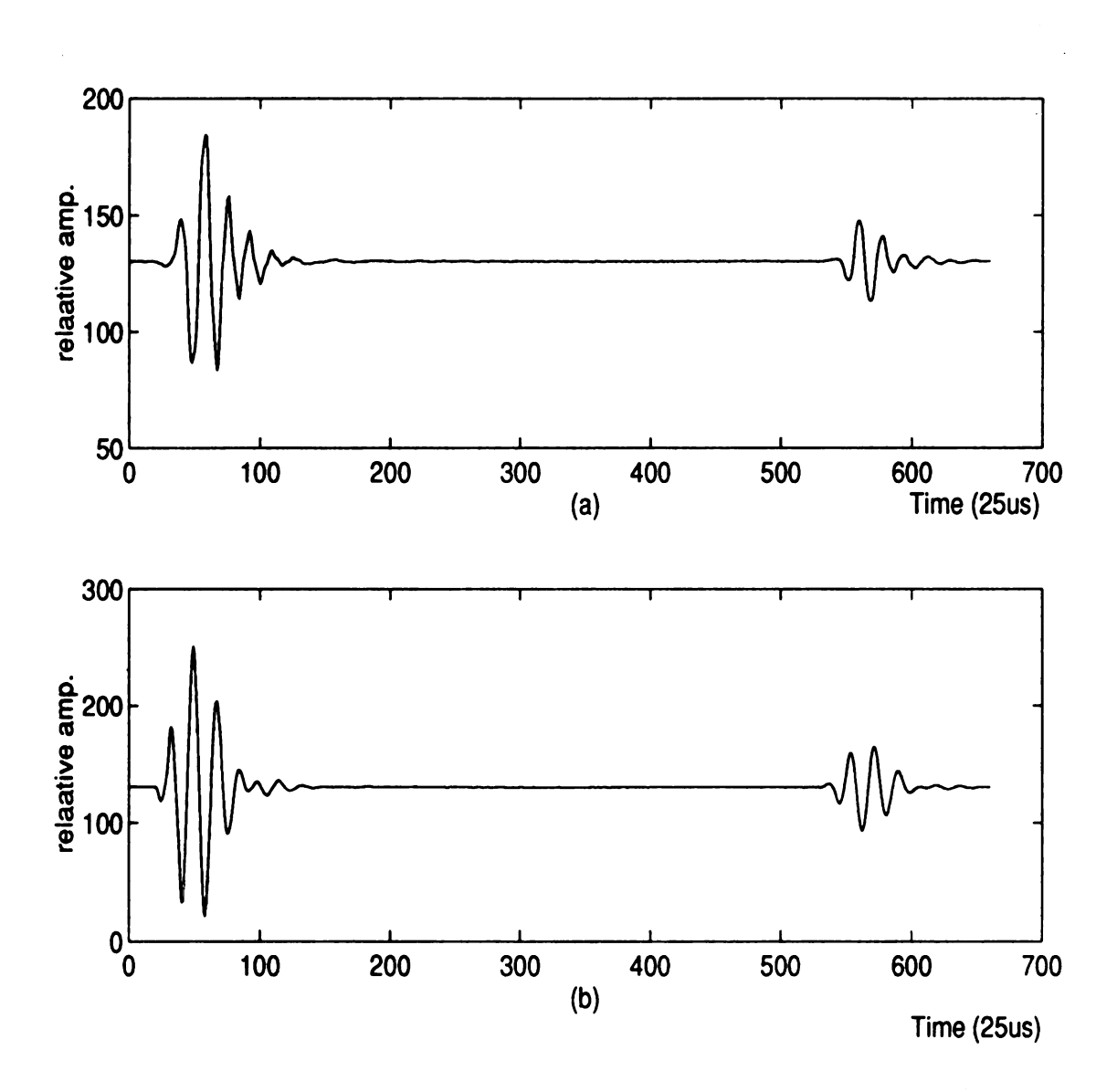


Figure 5.2. Reflection signals of single layer plexiglass in water. (a). Left-sided reflections. (b). Right-sided reflections.

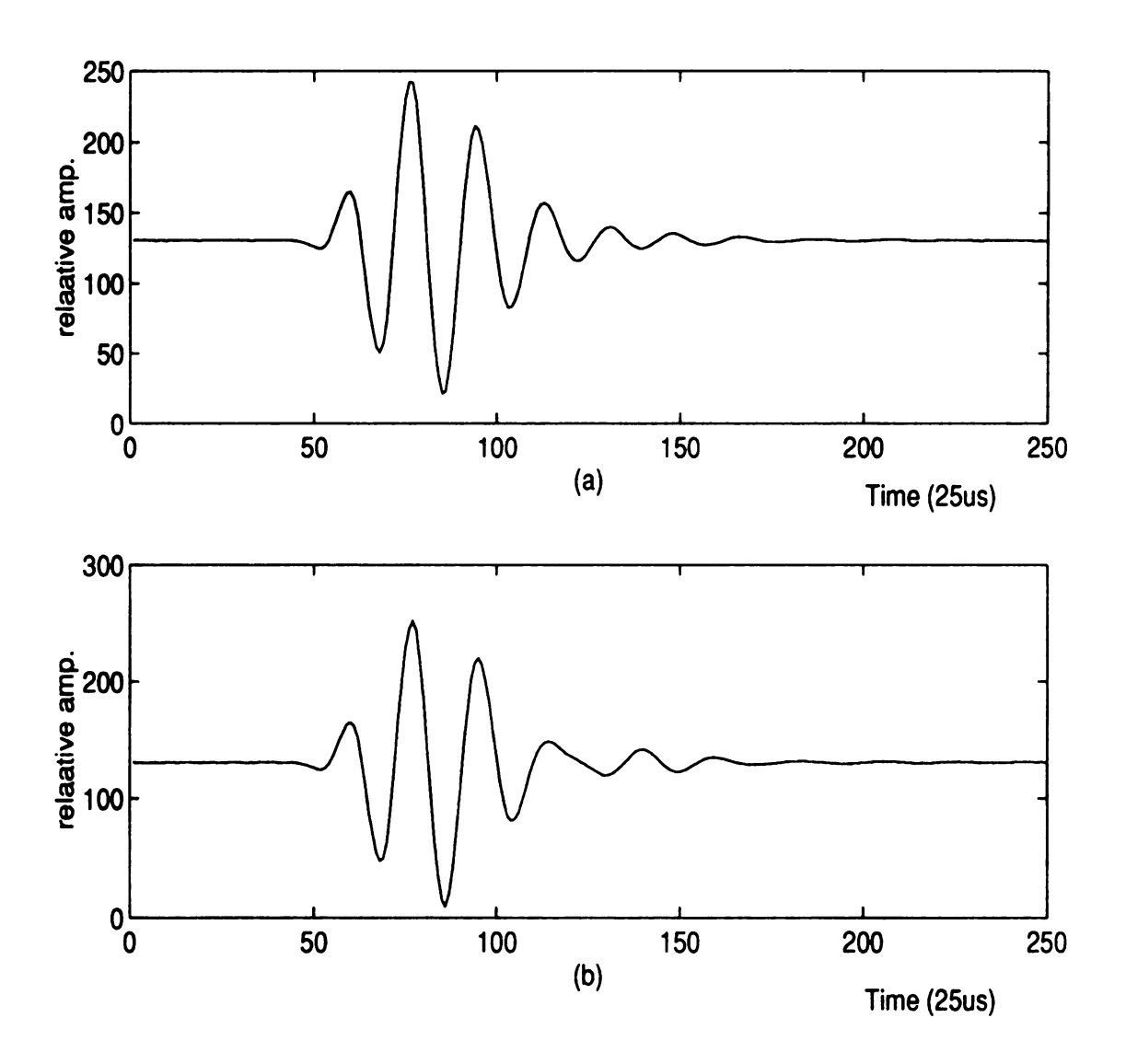


Figure 5.3. Transmission signals of single layer plexiglass in water. (a). Left to right transmission signal. (b). Right to left transmission signal.

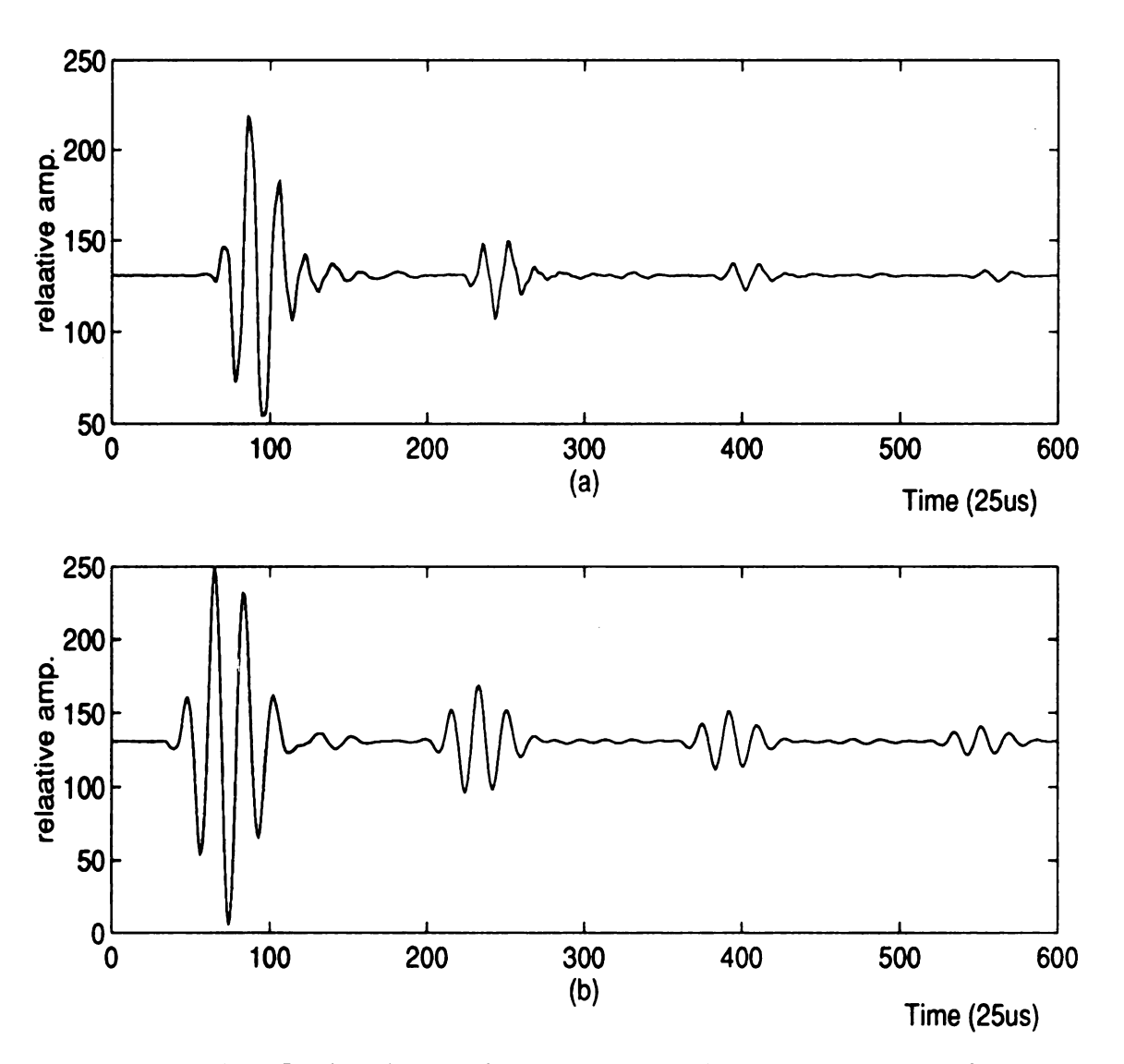


Figure 5.4. Reflection signals of single layer aluminum in water. (a). Left-sided reflection signal. (b). Right-sided reflection signal.

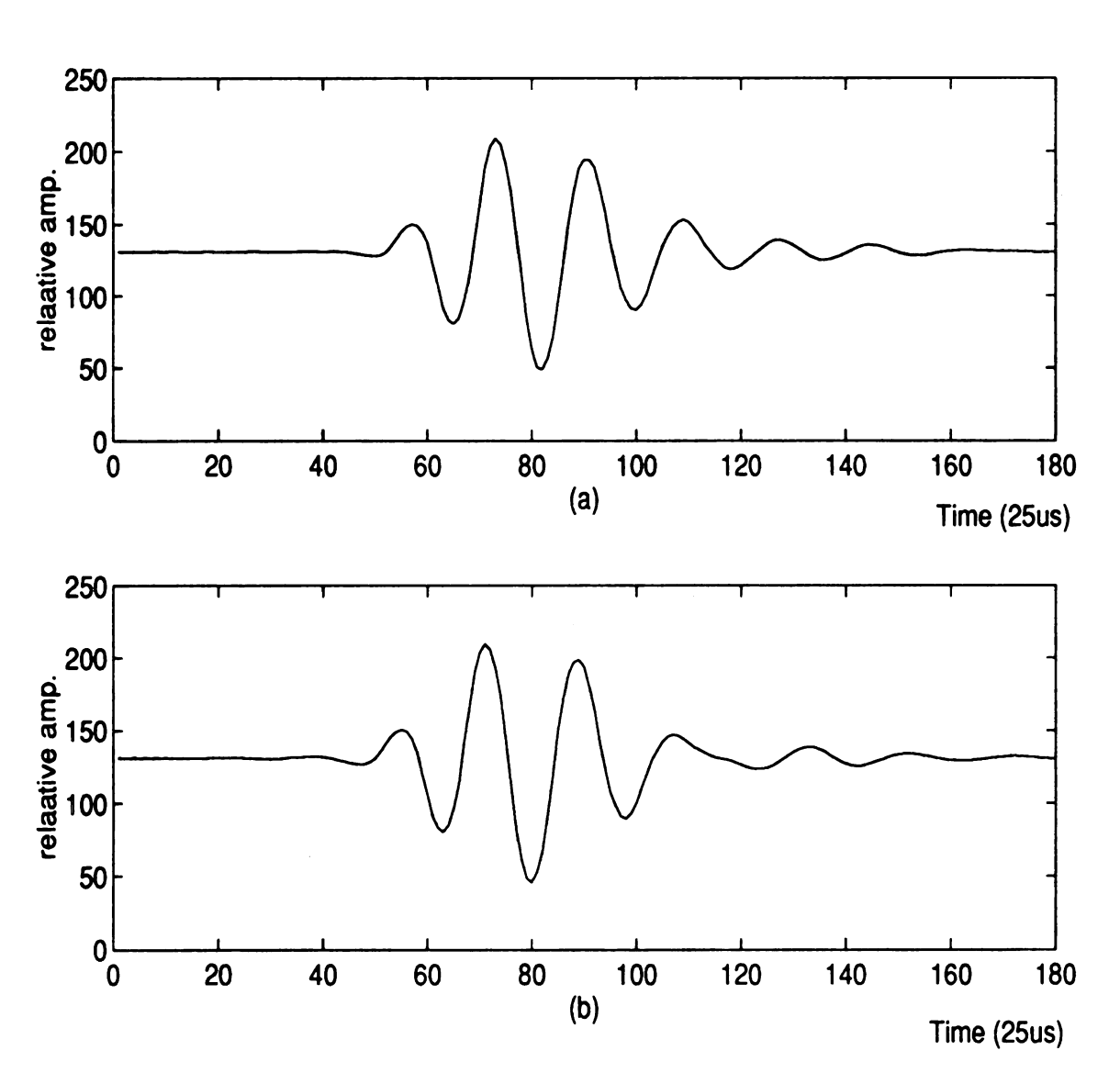


Figure 5.5. Transmission signals of single layer aluminum in water. (a). Left to right transmission signal. (b). Right to left transmission signal.

of the experimental results. The thickness of plexiglass and aluminum are 17.02 ±0.01 mm and 12.70 ±0.01 mm respectively. The received signals, two reflected signals and two transmission signals, from both sides are shown in Fig. 5.2 to Fig. 5.5. The signals were averaged 21 times to improve the signal-to-noise ratio. The impulse responses of the test medium are determined by locating the peak amplitudes of each echo and their corresponding traveling time. The algorithm of peak detection and traveling time determination is implemented in c language and listed in Appendix A. According to the Eq. 3.8 and Eq. 3.10. the estimated results of reflection coefficients and attenuation-velocity product of each layer were calculated and are shown in Table 5.1 and Table 5.2 for plexiglass and aluminum respectively.

From the reflection signals of aluminum (with high reflection coefficient) on both sides, the multiple reflections can be easily distinguished from the primary echo signals. As described in chapter 3, the multiple reflections of the same layer have properties of equal traveling time and have same polar sign as the primary echo of same side (have opposite polar sign to the primary echo of another side). The multiple reflections were detected and eliminated by our algorithm and are shown in Figure 5.6.

TABLE 5.1 Single layer of plexiglass (W-P-W), Thickness = 17.02±0.01 mm,

Parameters	Experimental results	Published Data*	Error(%)
rl	0.329	0.368	3.26%
r2	0.323	0.368	0.54%
αν (nepers/sec)	138,575.26	138,850	0.2%
v (m/sec)	2654.19	2680	0.96%
α (nepers/m)	52.21	51.81	0.77%

TABLE 5.2 Single layer of aluminum (W-A-W), Thickness = 12.70±0.01 mm.

Parameters	Experimental results	Published Data*	Error(%)
rl	0.847	0.848	1.06%
r2	0.841	0.848	3.07%
αν (nepers/sec)	3246.14	2984.32	8.77%
v (m/sec)	6369.97	6400	0.47%
α (nepers/m)	0.5096	0.4663	9.28%

For the multi-layered case, a model with two plexiglass layers separated by a layer of water was examined. The thickness of each layer is: layer I (1 = 11.02 mm), layer II (1 = 9.25 mm), and layer III (1 = 17.02 mm). The setup and the received signals from both sides are shown in Fig 5.6 and Fig. 5.7. Again, all signals are averaged 21 times to increase the signal-to-noise ratio. From the peaks of these echoes and the traveling time of each echo, the results can be obtained and were shown in Table 5.3.

The experimental results compared well with the published data. We noticed that the reflection coefficients in all cases are slightly smaller than the published data, while the attenuation coefficients are slightly larger. This is possibly due to the fact that there exist diffraction at each interface (deviated from normal incidence). The scattered energy will not be captured by the receiving transducer. In theory, any energy loss is considered to be attenuated (absorbed) by the medium. Unfortunately, the scattering effect is cumulative. It will be very pronounced as the number of layers increases. The experimental results of the multiple-layer structure demonstrates this effect. One of the drawbacks of this technique is the error accumulation. That is, if acoustic parameters of the first layer on both sides are not evaluated accurately, the errors will be propagating through the rest of process. To minimize this effect, the alignment of the transducers becomes very critical. Other drawbacks of this techniques were discussed in chapter 2.

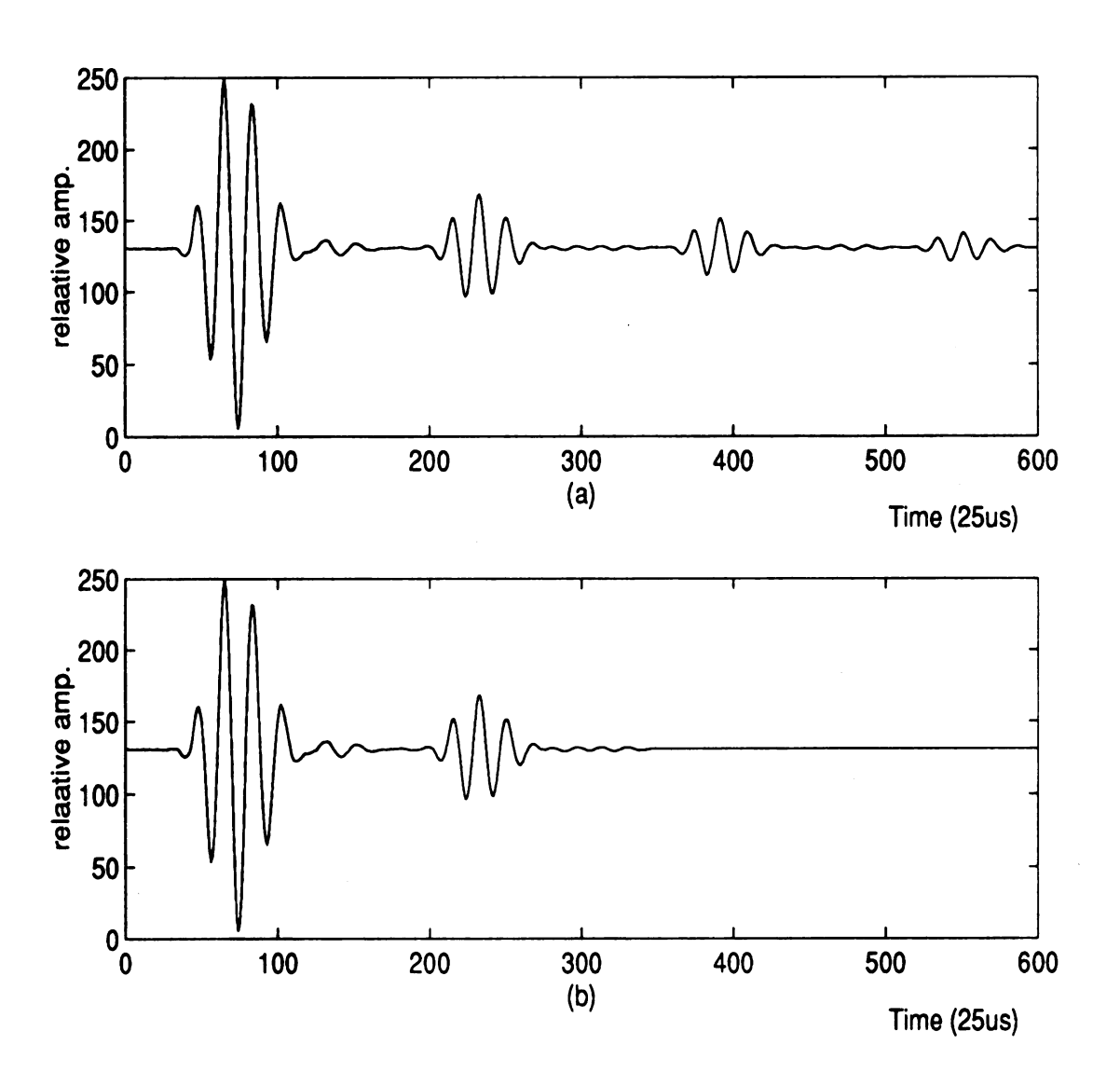


Figure 5.6. Multiple reflections elimination. (a). Left-sided reflections. (b). Left-sided signals after multiple elimination.

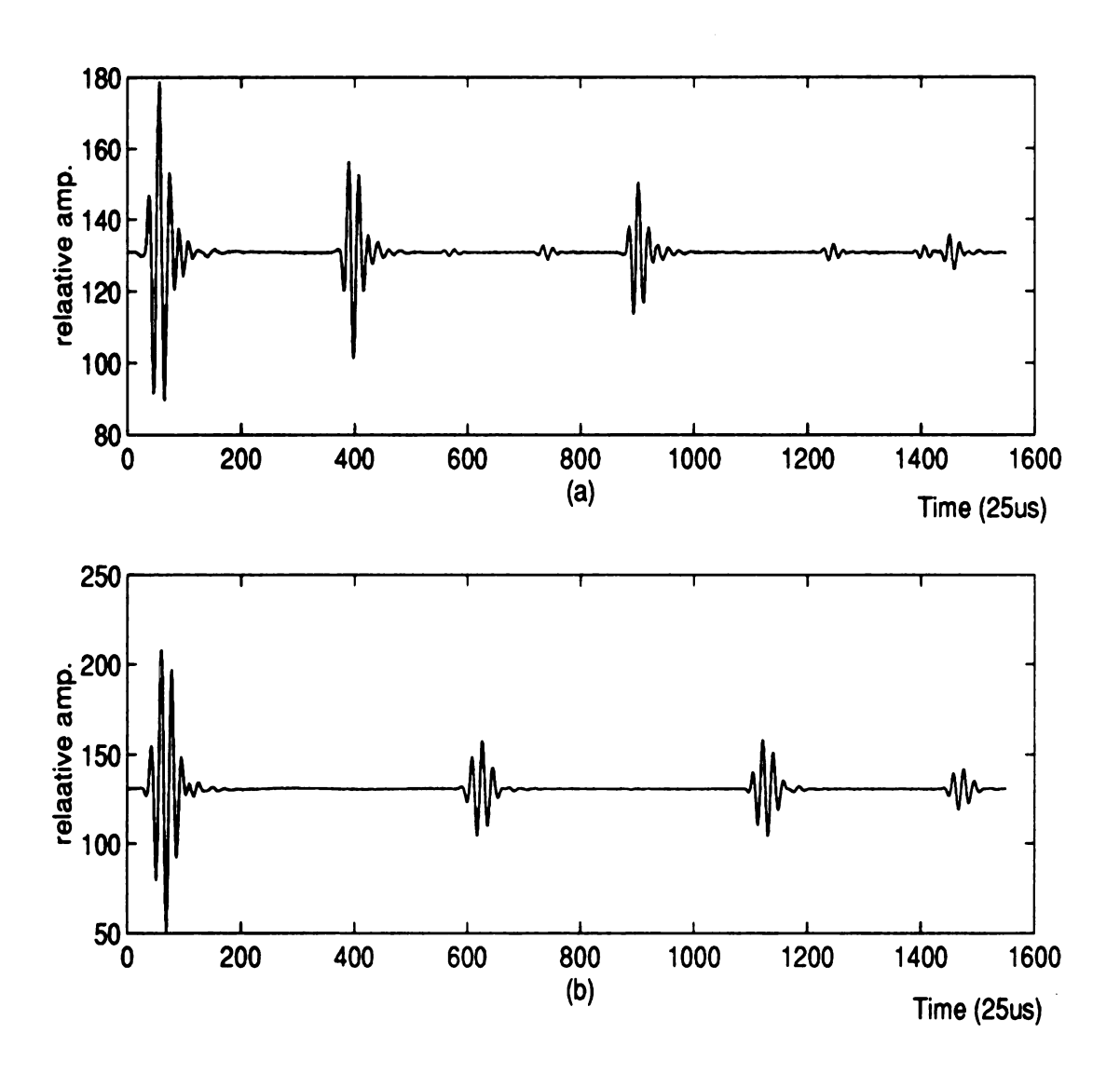


Figure 5.7. Reflection signals of multi-layered model. (a). Left-side reflections. (b). Right-sided reflections.

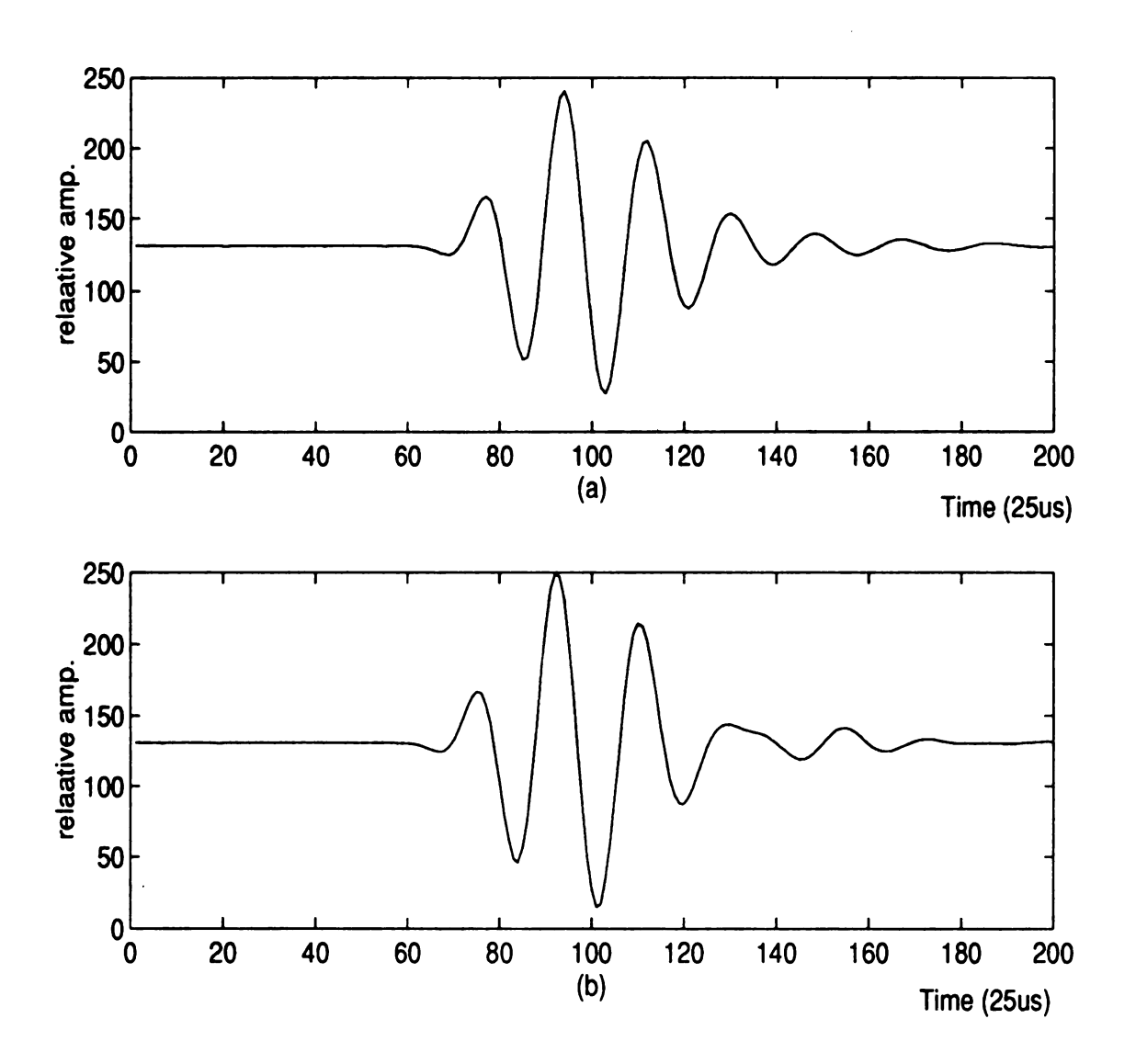


Figure 5.8. Transmission signals of multi-layered model. (a). Left to right transmission signal. (b). Right to left transmission signal.

TABLE 5.3 Three layers, plexiglass-water-plexiglass (W-P-W-P-W), Thickness: 11.02, 9.25, 17.02 ± 0.01 mm.

Parameters	Experimental results	Published Data*	Error(%)	
rl	0.319	0.368	12.8%	
r2	0.336	0.368	8.7%	
r3	0.323	0.368	12.2%	
r4	0.367	0.368	0.3%	
$\alpha_1 v_1$ (nepers/sec)	143,799.12	138,850	3.56%	
$\alpha_3 \nu_3$ (nepers/sec)	124,003.75	138,850	10.69%	
v1 (m/sec)	2663.44	2680	0.62%	
v3 (m/sec)	2654.19	2680	0.96%	
α ₁ (nepers/m)	53.99	51.81	4.2%	
α ₃ (nepers/m)	46.72	51.81	9.8%	

5.2 Comparison of two algorithms and two indices

In this section, two algorithms and two indices described in the previous chapter were compared using Monte Carlo study. Two experiments were conducted to get statistical results of the algorithms and indices over different data sets. First, an experiment for strongly clustered (well-clustered) data was performed. Then, an experiment for loosely clustered (weak-clustered) data was conducted. These two experiments are designed to test the clustering ability of the algorithms and cluster validity ability of the two indices to the clustered data.

Data generation

Clustered data were generated by the modified algorithm [87] of the Neyman-Scott [98] process in which spherically shaped Gaussian clusters are located randomly in the sampling window. This algorithm ensures that the clusters do not overlap more than a specified amount, provides for a minimum number of point per cluster, and permits the exact number of clusters to be specified. The details of the algorithm is described in [87]. Two important parameters, the spread of cluster (σ) and the overlap (I) between clusters are used to defined the generated data. Strongly clustered data has $\sigma = 0.01$ and I = 0.1, while the loosely clustered data has $\sigma = 0.1$ and I = 0.3. A spherical sampling window is a hypersphere whose radius is adjusted in each dimension to provide a volume of one.

Two experiments were performed to test two unsupervised learning (clustering) methods, the modified frequency sensitive competitive learning (MFSCL) and modified kmeans (MK), and two indices, S and MH.

Experiment I

This experiment estimates the number of clusters in a well-clustered data set with a hyperspherical sampling window. Since any reasonable estimator for the number of

79

clusters should work well for the well-clustered data, this experiment checks the

performance of two indices under almost ideal conditions. The experimental factors are

defined as following.

Sample size: { 100 }

Number of dimensions: $\{2, 3, 4, 5\}$

Number of clusters: { 2, 4, 6, 8}

Clustering method: { MFSCL, MK}

Sampling window: { Sphere }

Index: { S, MH}

These factors define 64 cells of experiment. Each cell was replicated 100 times.

Table 5.4. and Table 5.5 provides the raw results for the experiment I. From the Tables, the

MH index show better estimation results than that of S index under MFSCL method. The

S index is likely to underestimate the number of clusters. In all Tables, the cluster error is

defined by

cluster error = number of estimated clusters - true clusters.

Experiment II

This experiment compares the performance of the algorithms and the indices with

 $\sigma = 0.1$ and I = 0.3 data sets. The clusters of generated data are basically loose and

overlap with each other. The factors of experiment is defined as following.

Sample size: { 100 }

Number of dimensions: $\{2, 3, 4, 5\}$

Number of clusters: { 2, 4, 6, 8}

Clustering method: { MFSCL, MK}

80

Sampling window: { Sphere }

Index: { S, MH}

Again, the experiment has 64 cells. Each cell was replicated 100 times. The errors increased dramatically from those of previous results. The number of errors increased as the number of true clusters increased and as the dimensionality decreased and both indices tend to underestimate the number of clusters. The results are shown in the Table 5.6 and Table 5.7.

Both indices and algorithms performed well for the well-clustered data, the S index has a 88% recognition rate and the MH index has a 96% recognition rate. Neither index performed well with the weak-clustered data; S index has recognition rate of 28% and MH index has 42% recognition rate. The MH index has higher reliability and provides better results than those of the S index for both algorithms. Also, these results agree with those of Milligan and Cooper [95] and those of Jain and Dubes [87]. Thus, the MH index and the MFSCL were chosen in our application of ultrasonic material characterization.

TABLE 5.4 Errors in estimating number of clusters using S, 100 patterns, spread=0.01, overlap= 0.1, spherical window.

	,			p= 01.	i, spilerical v			,
Methods								
	Error	-3	-2	-1	0	1	2	>=3
	Dim.				2 clusters			
MK	2	0	0	10	90	0	0	0
	3	0	0	6	94	0	0	0
	4	0	0	2	98	0	0	0
	5	0	0	1	99	0	0	0
MFSCL	2	0	0	10	90	0	0	0
	3	0	0	6	94	0	0	0
	4	0	0	5	95	0	0	0
	5	0	0	3	97	0	0	0
					4 clusters			
MK	2	0	0	14	86	0	0	0
	3	0	0	4	96	0	0	0
	4	0	0	3	97	0	0	0
	5	0	0	0	100	0	0	0
MFSCL	2	0	0	12	88	0	0	0
	3	0	0	4	96	0	0	0
	4	0	0	2	98	0	0	0
	5	0	0	0	100	0	0	0
					6 clusters			
MK	2	2	4	21	73	0	0	0
	3	0	0	9	91	0	0	0
	4	0	0	3	97	0	0	0
	5	0	0	1	99	0	0	0
MFSCL	2	1	4	20	75	0	0	0
	3	0	2	5	93	0	0	0
	4	0	0	3	97	0	0	0
	5	0	0	0	100	0	0	0
					8 clusters			
MK	2	2	4	36	58	0	0	0
	3	0	0	11	85	0	0	0
	4	0	0	3	97	0	0	0
	5	0	0	1	99	0	0	0
MFSCL	2	0	9	35	56	0	0	0
	3	0	0	6	94	0	0	0
	4	0	0	2	98	0	0	0
	5	0	0	0	100	0	0	0

TABLE 5.5 Errors in estimating number of clusters using MH, 100 patterns, spread=0.01, overlap= 0.1, spherical window.

		Spi cau-						
Methods								,
	Error	-3	-2	-1	0	1	2	>=3
	Dim.				2 clusters			
MK	2	0	0	0	84	2	4	10
	3	0	0	0	96	1	0	3
	4	0	0	0	98	0	0	2
	5	0	0	0	100	0	0	0
MFSCL	2	0	0	0	94	0	0	6
	3	0	0	0	99	0	0	1
	4	0	0	0	100	0	0	0
	5	0	0	0	100	0	0	0
					4 clusters			
MK	2	0	0	2	97	0	0	0
	3	0	0	1	99	0	0	0
	4	0	0	0	100	0	0	0
	5	0	0	0	100	0	0	0
MFSCL	2	0	0	0	100	0	0	0
	3	0	0	0	100	0	0	0
	4	0	0	0	100	0	0	0
	5	0	0	0	100	0	0	0
					6 clusters			
MK	2	0	0	9	87	4	0	0
	3	0	0	3	97	0	0	0
	4	0	0	0	100	0	0	0
	5	0	0	0	100	0	0	0
MFSCL	2	0	0	5	95	0	0	0
	3	0	0	0	100	0	0	0
	4	0	0	0	100	0	0	0
	5	0	0	0	100	0	0	0
				0	8 clusters			
MK	2	0	0	12	85	2	0	1
	3	0	0	0	100	0	0	0
	4	0	0	0	100	0	0	0
	5	0	0	0	100	0	0	0
MFSCL	2	0	0	7	93	0	0	0
	3	0	1	1	98	0	0	0
	4	0	0	1	99	0	0	0
	5	0	0	0	100	0	0	0

TABLE 5.6 Errors in estimating number of clusters using S, 100 patterns, spread=0.1, overlap= 0.3, spherical window.

					, spilet Kai w			
Methods								
	Error	-3	-2	-1	0	1	2	>=3
	Dim.				2 clusters			
MK	2	0	0	29	30	11	10	20
	3	0	0	31	27	14	8	20
	4	0	0	29	34	16	5	16
	5	0	0	37	35	6	9	13
MFSCL	2	0	0	19	51	0	1	29
	3	0	0	13	82	1	1	3
	4	0	0	14	84	2	0	0
	5	0	0	17	83	0	0	0
					4 clusters			
MK	2	15	12	14	11	5	7	36
	3	5	8	17	19	13	1	37
	4	9	5	21	15	17	8	25
	5	1	8	13	20	14	15	29
MFSCL	2	25	9	36	21	2	2	7
	3	15	13	43	26	3	0	0
	4	23	4	29	41	2	0	1
	5	14	2	31	49	4	0	0
					6 clusters			
MK	2	23	4	9	11	8	8	37
	3	12	8	8	12	14	11	35
	4	7	10	9	8	9	16	41
	5	6	7	5	12	14	7	49
MFSCL	2	48	27	8	3	4	0	10
	3	28	26	22	19	2	1	2
	4	14	30	31	20	4	0	1
	5	10	18	39	31	0	0	0
					8 clusters			
MK	2	25	15	4	6	10	7	33
	3	26	8	5	8	9	6	39
	4	12	5	4	13	7	14	35
	5	8	5	6	5	16	7	53
MFSCL	2	74	5	5	4	1	2	9
	3	59	24	12	3	1	3	0
	4	34	26	25	10	2	3	0
	5	20	22	28	22	4	3	1

TABLE 5.7 Errors in estimating number of clusters using MH, 100 patterns, spread=0.1, overlap= 0.3, spherical window.

	1	7		Y			· · · · · · · · · · · · · · · · · · ·	
Methods								
	Error	-3	-2	-1	0	1	2	>=3
	Dim.				2 clusters			
MK	2	0	0	22	43	4	1	36
	3	0	0	15	62	3	4	16
	4	0	0	6	78	6	2	8
	5	0	0	6	83	4	3	4
MFSCL	2	0	0	0	32	7	8	53
	3	0	0	0	67	4	3	26
	4	0	0	0	82	4	4	10
	5	0	0	0	88	1	1	16
					4 clusters			
MK	2	5	13	10	5	6	13	48
	3	5	8	25	18	7	9	28
	4	3	4	23	29	11	8	19
	5	0	3	13	37	13	12	22
MFSCL	2	0	0	28	37	14	11	10
	3	0	4	22	61	7	3	3
	4	0	1	12	78	4	1	4
1	5	0	2	9	85	3	0	1
_					6 clusters			
MK	2	22	8	6	5	10	4	45
	3	17	9	6	8	10	9	40
	4	11	7	14 .	11	18	10	29
	5	3	7	20	20	9	10	31
MFSCL	2	4	16	28	30	11	9	4
	3	6	12	30	45	5	1	1
	4	7	11	20	59	3	0	0
	5	2	10	18	67	2	1	0
					8 clusters			
MK	2	21	5	5	11	15	14	29
	3	37	5	9	10	11	7	21
	4	20	12	12	17	5	15	19
	5	10	8	12	20	13	19	18
MFSCL	2	35	28	17	11	2	5	2
	3	28	23	19	16	7	6	4
	4	17	20	34	25	3	1	0
	5	13	17	28	29	3	0	6

5.3 Ultrasonic material characterization

In order to test the proposed method, several synthetic data sets and a well-known data set 'iris' were used. Then, a test phantom containing four different materials is scanned by our acoustic imaging system and the data set is used for material characterization. Finally, a slice of brain sample was examed.

To test the ability of pattern classification, a weakly clustered data set and a well separated data set both containing two features, four clusters and 50 patterns per cluster are presented to the neural network. These data sets are shown in Figs. 4.6(c) and 4.6(d). The clustering results are verified by MH versus number of clusters plot as shown in Fig. 5.9. The plot shows the significant knees of both cases occurred at an optimal number of clusters, i.e., four clusters. Then, the well-known test data set 'iris' was used. This four-feature data set contains three categories of iris and each category has 50 data patterns. The clustering result, shown in Fig. 5.9, suggests the desirable number of clusters for the given data set.

A test phantom which contains four different materials (plexiglass, aluminum, lead, and copper) with same thickness (6.24±0.01 mm) as shown in Fig. 5.10(a) is scanned by our acoustic scanning system. A area of 60 mm by 40 mm of the sample is scanned with step resolution of 1 mm. The structure arrangement of the phantom is shown in Fig. 5.10. Five features are extracted from the echo return of the phantom. The dependency between features is shown by eigenvector projection of the five features onto two-dimensional space, as shown in Fig. 5.11. Two of the five features, peak frequency and total energy, are discarded due to their strong dependency to central frequency and correlation coefficient respectively. The reduced 3-feature data set is then presented to the clustering network. Fig. 5.9 shows the clustering result. Fig 5.12 (a) shows the traditional acoustic C-scan image. Figs. 5.12 (b)-(d) demonstrate the images reconstructed from clustering information using different number of clusters. Notice that different color shades represent different

types of materials. With four clusters, the different types of materials (plexiglass, aluminum, lead, and copper) are being differentiated (different color shades). To see the ability of the system in retrieving information from multi-layered structure, a homogeneous material was placed between the target and the transducer. A 3.25 mm plexiglass plate was placed on top of the phantom. Fig. 5.13(a) shows the traditional acoustic C-scan image. Figs. 5.13(b)-(d) show the images resulted from clustering information using different number of clusters. The results are practically the same as those without the plexiglass plate in place. This indicates that the technique proposed can be used to identify materials inside a structure as well as being exposed. For the simulation data sets and the four-material phantom, the proposed method performs well distinguishing various materials. The computation time of the clustering process is in the order of tens of seconds to few minutes on the SUN SPARC station IPX.

Finally, a slice of human brain sample with hemorrhaged tumor, as shown in Fig. 5.14, was used. The clustering result suggests that separate the data set into four clusters is the best and is shown in Fig. 5.9. The C-scan and reconstructed images from the clustering information are shown in Fig. 5.15. Fig 5.15(a) shows the C-scan image. Fig. 5.15(b)-(f) depict the images reconstructed from clustering information using different number of clusters.

For the simulation data and the material phantom, the proposed method performs well and materials were classified as expected. For the hemorrhaged tumor brain sample, the clustering results do show the abnormal tissue portion. However, a detail identification of the brain sample requires further investigation for conclusive results. On the other hand, experts should joint and contribute their knowledge to the system while the system is examining amount of samples. The computation time of the clustering process for the brain sample is in the range of tens of minutes for our example.

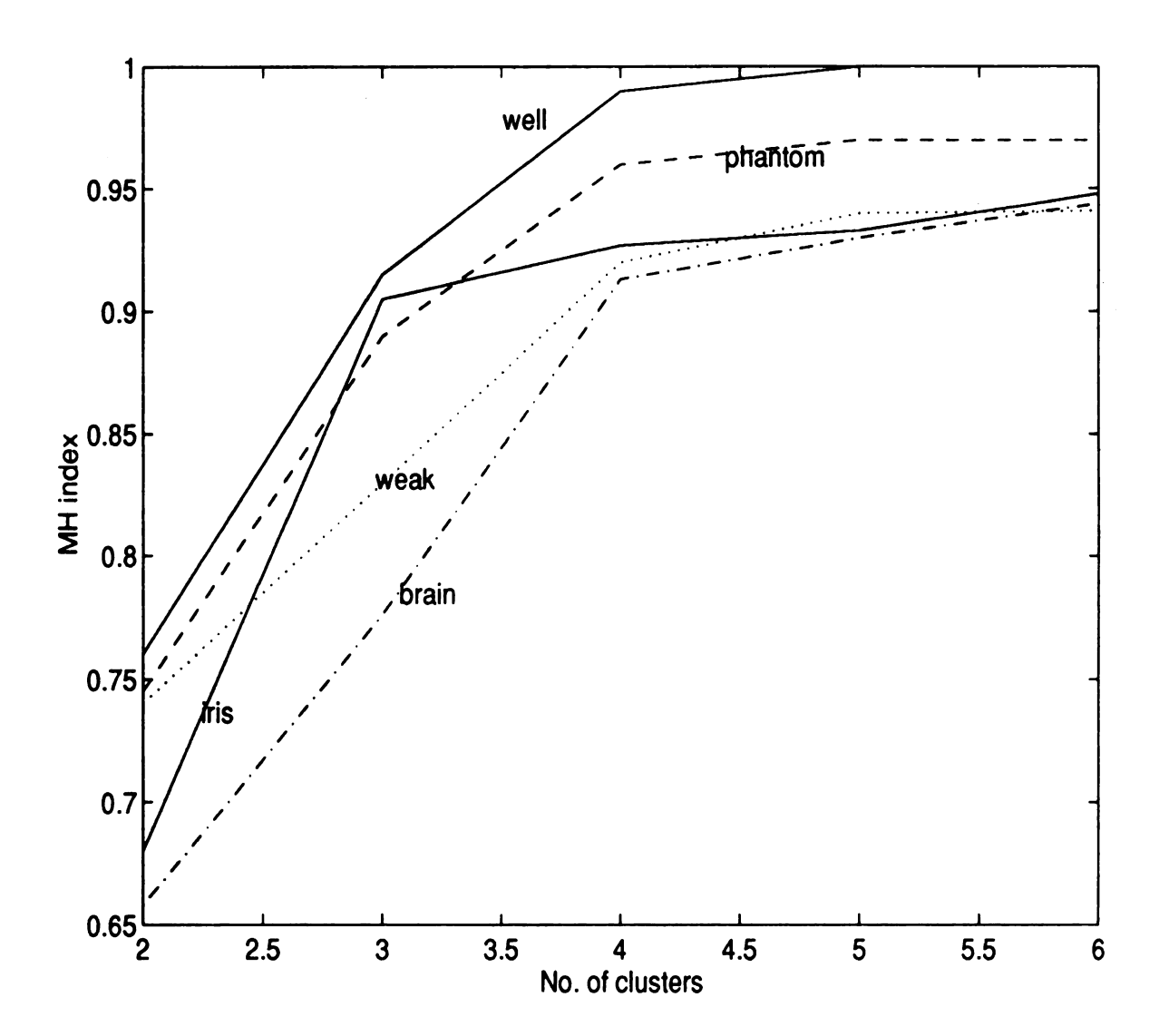
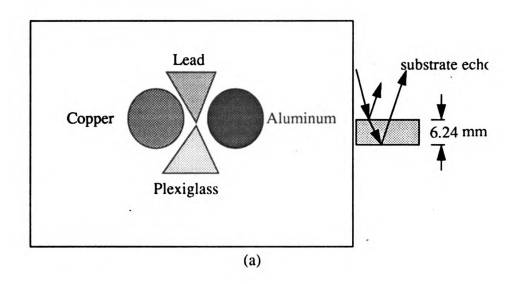


Figure 5.9. Modified Hubert's Gamma index v.s. number of clusters plots for different data sets.



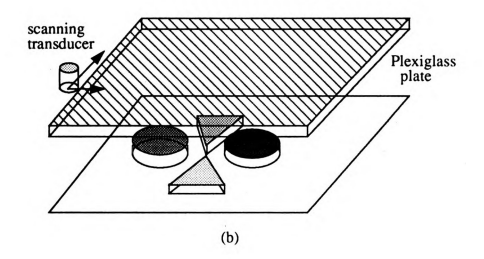


Figure 5.10 (a). Top view of phantom. (b). Phantom covered with plexiglass plate.

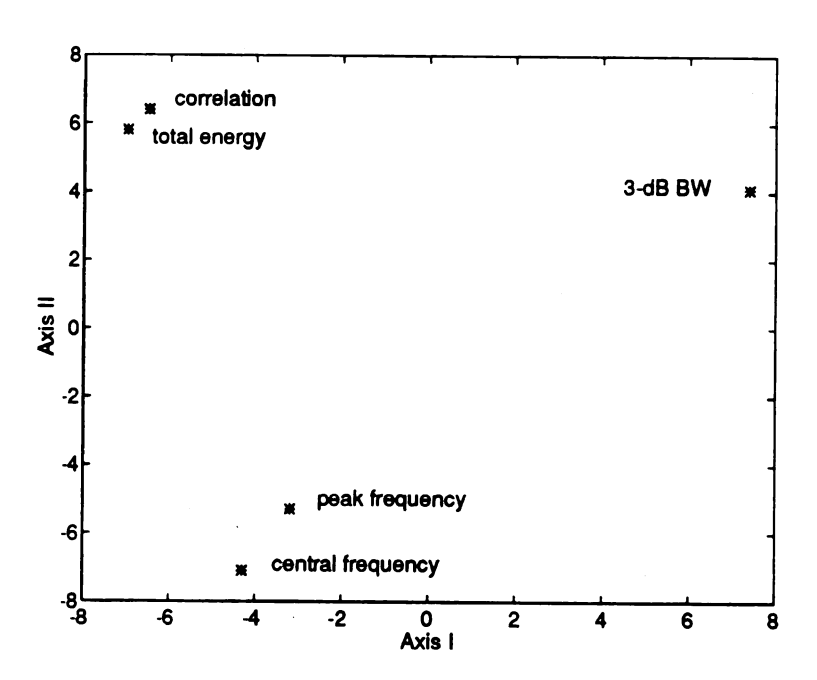
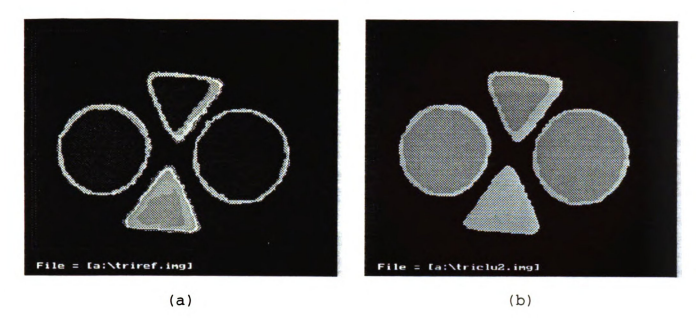


Figure 5.11. Linear (eigenvector) projection of five features onto two-dimensional space.



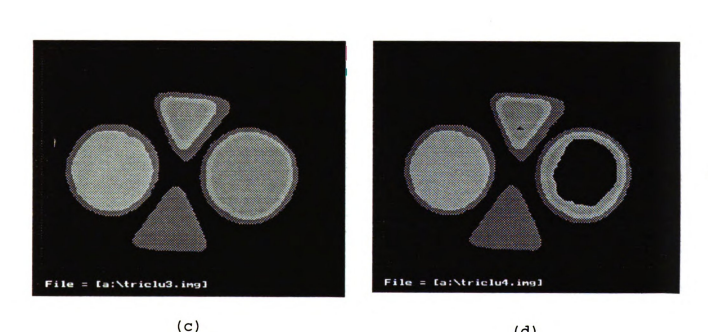
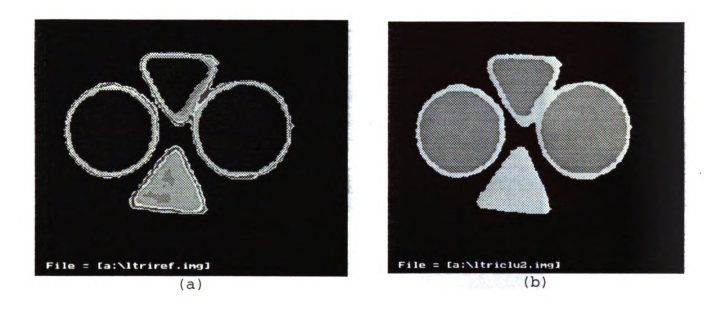


Figure 5.12. Images of phantom. (a). C-scan image. (b). Reconstructed image when segmented data set into two clusters. (c). Three clusters. (d). Four clusters. Different colors represent different clusters.

(d)



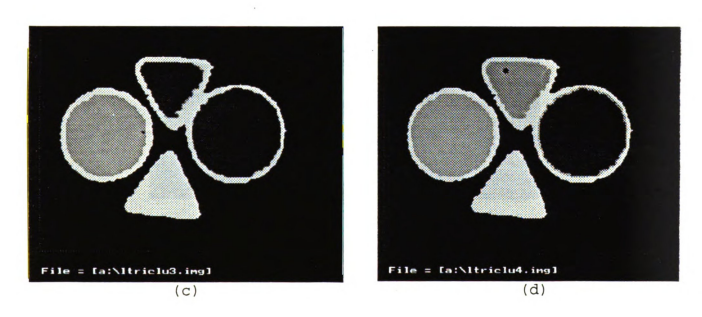


Figure 5.13. Images of phantom covered with plexiglass plate. (a). C-scan image. (b).

Reconstructed image when segmented data set into two clusters. (c). Three clusters. (d). Four clusters. Different colors represent different clusters.



Figure 5.14. Picture of human brain sample with hemorrhaged tumor.

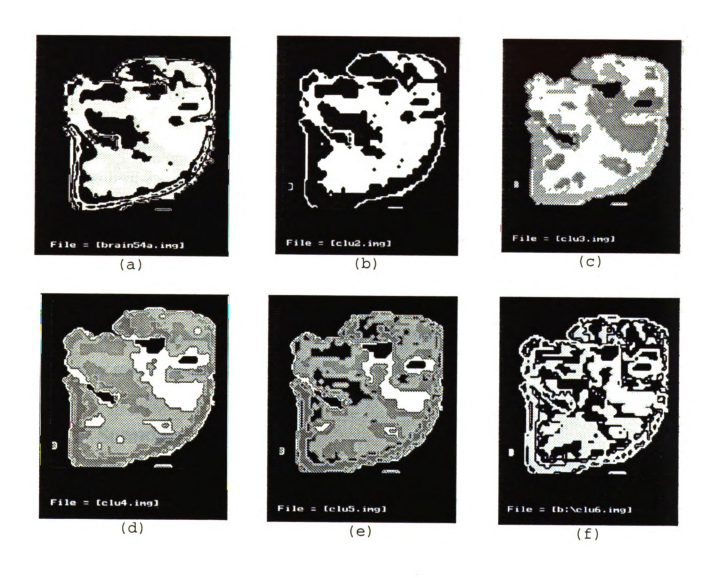


Figure 5.15. Images of human brain sample with hemorrhaged tumor. (a). C-scan image. (b) Reconstructed image when segmented data set into two clusters. (c). Three clusters. (d). Four clusters. (e) Five clusters. (f). Six clusters.

Chapter 6

6.0 Conclusions

Ultrasound is a very useful tool in a wide variety of applications, such as nondestructive evaluation for composite materials and diagnosis in medical field. Due to the complexity of acoustic beam profile and the random nature of its interaction with scatters inside the investigated medium, conventional time domain and frequency domain methods suffer from some inherent limitations in many applications. This thesis presents an approach for ultrasonic material characterization. By utilizing many aspects of most of the echo information and features of artificial neural networks, the proposed method do achieve some results that conventional methods could not offer.

6.1 Summary

Some basic theory of linear acoustic waves have been reviewed. Time domain and frequency domain methods for acoustic parameters estimation were described. Their advantages and limitations were also discussed.

Unlike the traditional ultrasonic detection technique using A-mode signal directly for material characterization, the proposed approach is to extract features from the echoes and form the data pattern set. Then, artificial neural networks principle is employed to perform the task of unsupervised learning. The data pattern set is then fed to the

unsupervised learning mechanism to obtain the clustering information. Materials were therefore classified by the clustering results in the form of color images. Different colors represent different clusters (acoustic properties). To ensure the unsupervised learning algorithm is efficient and the clustering results are trustful, a Monte Carlo study was performed in order to have a statistic knowledge on different algorithms (MFSCL and MK) and the cluster validity indices (S and MH). Finally, an unsupervised learning algorithm (MFSCL) and a index (MH) were chosen to employ in the ultrasonic material characterization system. The results demonstrate the superior performance of our methodology over the traditional methods.

6.2 Future work

Some concerns about ultrasonic detection system in general are its clarity, accuracy and real-time capability. Among the line of this research work, there are some topics to be pursued in the future.

- (1). Hardware implementation: Most of the processing time of our system is consumed in carrying out tasks of signals processing and unsupervised learning. These are mainly implemented by software. The system performance can be speed up dramatically if hardware implementation is achieved.
- (2). transducer array: In stead of using the stepping motors to control the movement of a single transducer, by the use of transducer array triggered by the multiplex electronic circuitry will make the system more closer to real-time operation.
- (3). Clinical evaluation: To improve the accuracy in the clinical evaluation, two aspects of works should be explored. First, build a knowledge base of

acoustic response of various biological tissues by the help of medical experts. Second, perform a thorough study on the relationship between the acoustic frequency response and the size of scatters in the biological tissue. This will provide us wit better understanding of potential applications of our system in noninvasive detection in general.



BIBLOGRAPHY

- [1] R. Kuc, M. Schwartz, and L. V. Minsky, "Parametric estimation of the acoustic attenuation coefficient slope for soft tissue," IEEE Ultrasonics Symposium Proceedings, pp. 44-47, 1976.
- [2] C. B. Burckhardt, "Speckle in ultrasound B-mode scans," IEEE Transactions on Sonics and Ultrasonics, vol. SU-25, no. 1, pp. 1-6, Jan. 1978.
- [3] J. P. Jones, "Ultrasonic impediography and its application to tissue characterization," Recent Advances in Ultrasound in Biomedicine, pp. 131-154, 1979.
- [4] F. S. Foster and J. W. Hunt, "Transmission of ultrasound beams through human tissue-focussing and attenuation studies," Ultrasound in Medicine and Biology, vol. 5, pp. 257-268, August 1979.
- [5] M. Itoh and H. Yokoi, "A computer-aided three-dimensional display system for ultrasonic diagnosis of a breast tumour," Ultrasonics, vol. 41, pp. 261-268, Nov. 1979.
- [6] J. P. Greenleaf and R. C. Bahn, "Clinical imaging with transmissive ultrasonic computerized tomography," IEEE Transactions on Biomedical Engineering, vol. 28, pp. 177-185, 1981.
- [7] E. J. Farrell, "Backscatter and attenuation imaging from ultrasonic scanning in medicine," IBM Journal of Research and Development, vol. 26, no. 6,/ pp. 746-758, Nov. 1982.
- [8] E. D. Blodgett, P H. Johnston, and J. G. Miller, "Estimation attenuation in composite laminates using backscattered ultrasound," IEEE Ultrasonics Symposium Proceedings, pp. 748-753, 1984.
- [9] L. Landini, R. Sarnelli and F. Squartini, "Frequency-dependent attenuation in breast tissue characterization," Ultrasound in Medicine and Biology, vol. 11, no. 4, pp. 599-

- 603, August 1985.
- [10] P. S. Green and M. Arditi, "Ultrasound reflex transmission imaging," Ultrasonic Imaging vol. 7, pp. 201-214, 1985.
- [11] P. He and J. F. Greenleaf, "Application of stochastic analysis to ultrasonic echoes-Estimation of attenuation and tissue heterogeneity from peaks of echo envelope," Journal of Acoustical Society of America, vol. 79 (2), pp. 526-534, Feb. 1986.
- [12] K. J. Parker, "Attenuation measurement uncertainties caused by speckle statistics," Journal of Acoustical Society of America, vol 80 (3), pp. 727-734, Sep. 1986.
- [13] A. E. Yagle, "A fast layer stripping algorithm for reconstructing a lossy layered medium," Journal of Acoustic Society of America, vol. 82 (3), pp. 927-936, Sep. 1987.
- [14] T. E. Preuss and G. Clark, "Use of time-of-flight c-scanning for assessment of impact damage in composites," Composites, vol. 19, pp. 145-148, Mar. 1988.
- [15] K. J. Parker and M. E. Lyons, "Absorption and attenuation in soft tissues:I-Calibration and error analysis," IEEE Transactions on Ultrasonics, Ferroelectrics, and Frequency Control, vol. 35, no. 2, pp. 242-252, Mar. 1988.
- [16] D. Ensminger, "Ultrasonics-fundamentals, technology, applications," New York: Marcel Deckker, Inc., 2nd ed., 1988.
- [17] B. Ho, D. Ye, R. Zapp and N. H. Wang, "Three-dimensional damage assessment in composites by ultrasonic imaging techniques," 43rd annual conference of reinforced plastics and composites, 1988.
- [18] P. He, "On the estimation of acoustic attenuation coefficient from peaks of echo envelope," Journal of Acoustical Society of America, vol 83 (5), pp. 1919-1926, May, 1988.
- [19] H. S. Jang, T. K. Song and S. B. Park, "Ultrasound attenuation estimation in soft tissue using the entropy difference of pulsed echoes between two adjacent envelope segments," Ultrasonic Imaging vol. 7, pp. 248-264, 1988.
- [20] M. E. Lyons and K. J. Parker, "Absorption and attenuation in soft tissue II-Experimental results," IEEE Transactions on Ultrasonics, Ferroelectrics, and Frequency

- Control, vol. 35, no. 4, pp. 511-521, July 1988.
- [21] G. E. Sleefe and P. P. Lele, "Tissue Characterization based on scatterer number density estimation," IEEE Transactions on Ultrasonics, Ferroelectrics, and Frequency Control, vol. 35, no. 6, pp. 749-757, Nov. 1988.
- [22] K. J. Parker, R. M. Lerner and R. C. Waag, "Comparison of techniques for in vivo attenuation measurements," IEEE Transactions on Biomedical Engineering, vol. 35, no. 12, pp. 1064-1068, Dec. 1988
- [23] E. Walach, A. Shmulewitz, Y. Itzchak and Z. Heyman, "Local tissue attenuation images based on pulsed-echo ultrasound scans," IEEE Transactions on Biomedical Engineering vol. 36, no. 2, pp. 211-221, Feb. 1989.
- [24] G. Hayward and J. E. Lewis, "Comparison of some non-adaptive deconvolution techniques for resolution enhancement of ultrasonic data," Ultrasonics, vol. 27, pp. 155-164, May, 1989.
- [25] R. Momenan and etc., "Application of pattern recognition techniques in ultrasound tissue characterization," IEEE Engineering in Medicine and Biology Society 11th Annual International Conference, PP. 411-412, June, 1989.
- [26] J. Saniie and D. T. Nagle, "Pattern recognition in the ultrasonic imaging of reverberant multilayered structures," IEEE Transactions on Ultrasonics, Ferroelectrics, and Frequency Control, vol. 36, no. 1, pp. 80-92, Jan. 1989.
- [27] P. He, "Acoustic attenuation Estimation for soft tissue from ultrasound echo envelope peaks," IEEE Transactions on Ultrasonics, Ferroelectrics, and Frequency Control, vol. 36, no. 2, pp. 197-203, March 1989.
- [28] M. Nikoonahad and M. V. Iravani, "Focusing ultrasound in biological media," IEEE Transactions on Ultrasonics, Ferroelectrics, and Frequency Control, vol.36, no. 2, pp. 209-215, March 1989.
- [29] W. Sachse, B. Castagnede, I. Grabac, K. Y. Kim, and R. L. Weaver, "Recent developments in quantitative ultrasonic nde of composites," Ultrasonics, vol. 28, pp. 97-104, Mar. 1990.
- [30] D. L. Liu, "Sound velocity inversion in layered media with band-limited and noise-

- corrupted data," IEEE Transactions on Biomedical Engineering, vol. 38, no. 9. pp. 1042-1047, Oct. 1991.
- [31] L. Weng, J. M. Reid, P. M. Shankar and K. Soetanto, "Ultrasound speckle analysis based on the K distribution," Journal of Acoustical Society of America, vol 89 (6), pp. 2992-2995, June, 1991.
- [32] I. Beretsky and G. A. Farrel, "Improvement of ultrasonic imaging and media characterization by frequency domain deconvolution, experimental study with non-biological models," Ultrasound in Medicine, vol. 38, pp. 1645-1665, 1977.
- [33] J. P. Steiner, E. S. Furgason, and W. L. Weeks, "Robust deconvolution of correlation functions," IEEE ultrasonics Symposium Proceedings, pp 1031-1035, 1987.
- [34] A. Yamada, "On-line deconvolution for the high resolution ultrasonic pulse-echo measurement with narrow-band transducer," IEEE Ultrasonics Symposium Proceedings, pp. 1027-1030, 1987.
- [35] N. H. Wang, B. Ho, and R. Zapp, "Attenuation and velocity imagings of biological tissues by broadband ultrasonic signals," International Symposium on Ultrasonic Imaging and Tissue Characterization, June, 1990.
- [36] E. E. Hundt and E. A. Trautenberg, "Digital processing of ultrasonic data by deconvolution," IEEE Transactions on Sonics and Ultrasonics, vol. su-27, pp. 249-252. Sept. 1980.
- [37] A. Papoulis and C. Chazmas, "Improvement of range resolution by spectral extrapolation,"
- [38] J. W. Mimbs, M. O'Donnell, J. G. Miller, and B. E. Sobel, "Changes in ultrasonics attenuation indicative of early myocardium ischemic injury," American Journal of Physiology, vol. 236, pp. 340-344, 1979.
- [39] J. F. Greenleaf, J. Ylitalo, and J. J. Gisvold, "Ultrasonic computed tomography for breast examination," IEEE Engineering in Medicine and Biology Magazine, pp. 27-32, Dec. 1987.
- [40] G. H. Glover and J. C. Sharp, "Reconstruction of ultrasound propagation speed distributions in soft tissues: time-of-flight tomography," IEEE Transactions on Sonics

- and Ultrasonics, vol. su-24, NO. 4, pp. 229-234, July 1977.
- [41] R. Kuc, "Clinical application of an ultrasound attenuation coefficient estimation technique for liver pathology characterization," IEEE Transactions on Biomedical Engineering vol. BME-27, no. 6, pp. 312-319, June 1980.
- [42] P. A. Narayana and J. Ophir, "On the frequency dependence of attenuation in normal and fatty liver," IEEE Transactions on Sonics and Ultrasonics, vol. su-30, no. 6, pp. 379-383, Nov. 1983.
- [43] R. Kuc, "Estimating acoustic attenuation from reflected ultrasound signals: comparison of spectral-shift and spectral-difference approaches," IEEE Transaction on Acoustics Speech, and Signal Processing, vol. ASSP-32, no. 1, pp. 1-6, Freb. 1984.
- [44] P. A. Narayana, J. Ophir, and N. F. Maklad, "The attenuation of ultrasound in biological fluids," Journal of Acoustical Society of America, vol. 76 (1), pp. 1-4, July 1984.
- [45] R. Kuc, "Estimating reflected ultrasound spectra from quantized signals," IEEE Transactions on Biomedical Engineering vol. BME-32, no. 2, pp. 105-112, Freb. 1985.
- [46] J. Ophir, R. E. Mcwrite, N. F. Maklad, and P. M. Jaeger, "A narrowband pulse-echo technique for in Vivo ultrasound attenuation estimation," IEEE Transactions on Biomedical Engineering vol. BME-32, no. 3, pp. 205-212, March 1985.
- [47] R. Kuc, "Bounds on estimating the acoustic attenuation of small tissue regions from reflected ultrasound," IEEE proceedings, vol. 73, no. 7, pp. 1159-1168, July 1985.
- [48] F. L. Lizzi, M Ostromogilsky, E. J. Feleppa, and et. al., "Relationship of ultrasonic spectral parameters to features of tissue microstructure," IEEE Transactions on Ultrasonics, Ferroelectrics, and Frequency Control, vol. UFFC-33, no. 3, pp. 319-328, May 1986.
- [49] Y. Hayakawa, T. Wagai, K. Yosioka, and et. al., "Measurement of ultrasound attenuation coefficient by a multifrequency echo technique-theory and basic experiments," IEEE Transactions on Ultrasonics, Ferroelectrics, and Frequency Control, vol. UFFC-33, no. 6, pp. 759-764, Nov. 1986.

- [50] K. A. Dines and S. A. Goss, "Computed ultrasonic reflection tomography," IEEE Transactions on Ultrasonics, Ferroelectrics, and Frequency Control, vol. UFFC-34, no. 3, pp. 309-317, May 1987.
- [51] S. Finette, "Computational methods for simulating ultrasonic scattering in soft tissue," IEEE Transactions on Ultrasonics, Ferroelectrics, and Frequency Control, vol. UFFC-34, no. 3, pp. 283-292, May 1987.
- [52] S. Serbarian, "Influence of attenuation upon the frequency content of a stress wave packet in graphite," Journal of Acoustical Society of America, vol.42 (5), pp.1052-1159, April 1967.
- [53] T. Yokota and Y. Sato, "Super-resolution ultrasonic imaging by using adaptive focusing," Journal of Acoustical Society of America, vol. 77 (2), pp. 567-572, Feb. 1985.
- [54] J. Ophir, R. E. Mcwhirt, N. F. Maklad, and P. M. Jaeger, "A narrow band pulse-echo technique for in vivo ultrasonic attenuation estimation," IEEE Transaction on Biomedical Engineering, vol. BME-32, no. 3, pp. 205-212, March 1985.
- [55] I. Claesson, and G. Salomonsson, "Estimation of varying ultrasonic attenuation," Ultrasound in Medicine and Biology, vol. 11, pp. 131-145, 1985.
- [56] P. Karpur, P. M. Shankar, J. L. Rose and V. L. Newhouse, "Split spectrum processing: determination of variable bandwidth for spectral splitting," Ultrasonics vol. 26, pp. 204-209, July, 1988.
- [57] J. D. Aussel, "Split spectrum processing with finite impulse response filters of constant frequency-to-bandwidth ratios," Ultrasonics, pp. 630-641, July 1990.
- [58] J. L. Rose, P. Karpur and V. L. Newhouse, "Utility of split spectrum processing in ultrasonic nondestructive evaluation," Material Evaluation, vol. 46, pp. 14-22, Jan. 1988.
- [59] P. Schattner, T. K. Whitehurst, J. F. Jensen, A. S. Shah and P. S. Green, "Three-dimensional ultrasonic reflection and attenuation imaging," IEEE Transactions on Ultrasonics, Ferroelectrics, and Frequency Control, vol. 21, no. 1, pp. 102-111, Jan. 1992.
- [60] J. J. Hopfield and D. W. Tank, "Neural computation decisions in optimization problems," Biological Cybernetics, vol. 52, pp. 141-152, 1985.

- [61] D. W. Tank and J. J. Hopfield, "Simple neural optimization networks: An A/D converter, signal decision network, and a linear programming circuit," IEEE Transaction on Circuits and Systems, vol. CAS-33, no.5, pp. 533-541, 1986.
- [62] G. V. Wilson and G. S. Pawley, "On the stability of the TSP problem algorithm of Hopfiled and Tank," Biological Cybernetics 58, pp. 63-70, 1988.
- [63] C. Y. Maa, M. A. Shanblatt, "Stability of linear programming neural network for problems with hypercube feasible region," Proceedings of the IEEE International Conference on Neural Networks, San Diego, CA, June 1990.
- [64] M. P. Kennedy and L. O. Chua, "Neural Networks for nonlinear programming," IEEE Transaction on Circuits and Systems, vol. CAS-35, no.5, pp. 554-562, May, 1988.
- [65] W. Li and M. Nasrabadi, "Object recognition based on graph matching implemented by Hopfield-style neural network," Proceedings of IEEE International Conference on Neural Networks, Washington, DC, vol. II, pp. 287-290, June 1989.
- [66] A. Waibel, et al., "Phoneme recognition using time-delay neural networks," IEEE Transaction on ASSP, vol. 37, no. 3, March 1989.
- [67] C. R. Hill, "Physical principles of medical ultrasonics," Ellis Horwood Limited, England, 1986.
- [68] W. J. Fry and F. Dunn, "Ultrasound: Analysis and Experimental method in biological research," Physical Technique in Biological Research, vol. 4, Academic press, New York, pp. 261-314, 1962.
- [69] E. L. Madsen, H. J. Satkoff and J. A. Zagzebski, "Ultrasonic shear wave properties of soft tissue and tissuelike material," J. Acoust. Soc. Am. 74, pp. 1346-1355, 1983.
- [70] W. S. McCulloch and W. H. Pitts, "A logical calculus for the ideas immanent in nervous activity," Bulletin of Mathematical Biophysics, vol. 5, pp. 115-133, 1943.
- [71] H. Ritter and K. Schulten, "Kohonen's self-organizing maps: exploring their computational capabilities," IEEE International Conference on Neural Networks, San Diego, vol. I, pp. 109-116, 1988.
- [72] S. Kirkpatrick, C. D. Gelatt, and M. P. Vecchi, "Optimization by simulated anneal-

- ing," Science 220, pp. 671-680, 1983.
- [73] T. Kohonen, "Self-organization and associative memory," Berlin: Springer-Verlag, 1984.
- [74] B. Ho, N. H. Wang, M. Rich, and R. Zapp, "High range resolution ultrasonic imaging for evaluation of layered composite materials," 5th technical Conference of the American Society for Composites, 1990.
- [75] K. Matsuzawa, N. Inoue and T. Hasegawa, "A new simple method of ultrasonic velocity and attenuation measurement in a high absorption liquid," J. Acoust. Soc. Am., vol. 81 no. 4, pp. 947-951, 1987.
- [76] W. N. Mc Dicken, "Diagnostic ultrasonics," Churchill Livinston, 3 rd ed., 1991.
- [77] L. S. Wilson, D. E. Robinson and B. D. Doust, "Frequency domain processing for ultrasoic attenuation measurement in liver," Ultrasonic Imaging, 6, pp. 278-292, 1984.
- [78] B. HO, R. Zapp and T. S. Chen ,"Impedance and attenuation profile estimation of multi-layered material from reflected ultrasound," IEEE Trans. on Intrumentation and Measurement, Aug., 1991.
- [79] J. G. Miller, J. E. Perez, J. G. Mottley, E. I. Madaras, P. H. Johnston, E. D. Blodgett, L. J. Thomas III, and B. E. Sobel, "Myocardial tissue characterization: An approach based on quantitative backscatter and attenuation," Proceedings IEEE Ultrason., pp. 782-793, 1983.
- [80] J. Ophir, T. H. Shawker, N. F. Maklad, J. G. Miller, S. W. Flax, P. A. Narayana, and J. P. Jones, "Attenuation estimation in reflection: Progress and prospects," Ultrasonic Imaging, vol. 6, pp. 349-395, 1984.
- [81] R. Kuc, and D. P. Regula, Jr., "Diffraction effects in reflected ultrasound spectral estimates," IEEE Transaction on Biomedical Engineering, vol. BME-31, no. 8, pp. 537-545, Aug. 1984.
- [82] S. W. Flax, N. J. Pelc, G. H. Glover, F. D. Gutmann, and M. McLachlan, "Spectral characterization and attenuation measurement in ultrasound," Ultrasonic Imaging, vol. 5, pp. 95-116, 1983.

- [83] K. J. Parker and R. C. Waag, "Measurement of ultrasonic attenuation within regions selected from B-scan images," IEEE Transaction on Biomedical Engineering, vol. BME-30, no. 8, pp. 431-437, Aug. 1983.
- [84] L. S. Wilson, D. E. Robinson, and B. D. Doust, "Frequency domain processing for ultrasonic attenuation measurement in liver," Ultrasonic Imaging, vol. 6, pp. 278-292, 1984.
- [85] C. R. Crawford and A. C. Kak, "Multiples artifacts in ultrasonic transmission tomography," Purdue Univ., Lafayette, IN, Tech, Rep. TR-EE 81-43, Dec. 1981.
- [86] M. Fink, F. Hottier, and J. F. Gardoso, "Ultrasonic signal processing for in vivo attenuation measurement: short-time fourier analysis," Ultrasonic Imaging, vol. 5, pp. 117-135, April 1983.
- [87] R. C. Dubes and A. K. Jain, "Algorithms for clustering data," Prentice Hall, New Jersey, 1988.
- [88] P. R. Krishnaiah and L. N. Kanal, "Classification, pattern recognition, and reduction of dimensionality," Handbook of Statistics, Vol. 2, Amsterdam, North Holland, 1982.
- [89] J. H. Winters and C. Rose, "Minimum distance automata in parallel networks for Optimum classification," Neural Networks 2, pp. 127-132, 1989.
- [90] R. O. Duda and P. E. Hart., "Pattern classification and Scene analysis," NewYork: John Wiley and Sons, 1973.
- [91] S. Grossberg, "Adaptive pattern classification and universal recording: Part IParallel development and coding of neural feature detectors," *Biological Cybernetics* 23, 121-134, 1976.
- [92] S. Grossberg, "Competitive learning: From interactive activation to adaptive resonance," Cognitive Science 11, 23-63, 1987.
- [93] D. Desieno, "Adding a conscience to competitive learning," *IEEE International Conference on Neural Networks*, 1117-1124, 1988.
- [94] C. S Ahalt., K. A. Krishnamurphy, P. Chen. and E. D. Melton, "Competitivelearning for vector quantization," *Neural Networks* 3, 277-290, 1990.
- [95] G. W. Milligan and M. C. Cooper, "An examination of procedures for determining the number of clusters in a data set," *Psychometrika* 50, 159-179, 1985.

- [96] G. J. Hueter,"Sloution of the travelling salesman problem with an adaptive ring," IEEE International Conference on Neural Networks, vol. I, pp. 85-92, San Diego, 1988.
- [97] C. C. Chiu and M. A. Shanblatt, "Neural networks for dynamic programming," P.h. D. Dessertation, Michigan State Univ. College of Engr., 1991.
- [98] J. Neyman and E. L. Scott, "Processes of clustering and applications in stochastic point processes," Statistical Analysis, Theory, and Applications, John Wiley and Sons, New York, 1972.

MICHIGAN STATE UNIV. LIBRARIES
31293010154205